molecules

MDPI

Article

Poly(imidazolyliden-yl)borato Complexes of Tungsten: Mapping Steric vs. Electronic Features of *Facially* Coordinating Ligands

Callum M. Inglis, Richard A. Manzano, Ryan M. Kirk, Manab Sharma, Madeleine D. Stewart, Lachlan J. Watson and Anthony F. Hill *

Research School of Chemistry, Australian National University, Canberra, ACT 2601, Australia
* Correspondence: a.hill@anu.edu.au

Abstract: A convenient synthesis of $[HB(HImMe)_3](PF_6)_2$ (ImMe = *N*-methylimidazolyl) is decribed. This salt serves in situ as a precursor to the tris(imidazolylidenyl)borate $Li[HB(ImMe)_3]$ pro-ligand upon deprotonation with ^{n}BuLi. Reaction with $[W(\equiv CC_6H_4Me\text{-}4)(CO)_2(pic)_2(Br)]$ (pic = 4-picoline) affords the carbyne complex $[W(\equiv CC_6H_4Me\text{-}4)(CO)_2\{HB(ImMe)_3\}]$. Interrogation of experimental and computational data for this compound allow a ranking of familiar tripodal and facially coordinating ligands according to steric (percentage buried volume) and electronic (ν_{CO}) properties. The reaction of $[W(\equiv CC_6H_4Me\text{-}4)(CO)_2\{HB(ImMe)_3\}]$ with $[AuCl(SMe_2)]$ affords the heterobimetallic semi-bridging carbyne complex $[WAu(\mu\text{-}CC_6H_4Me\text{-}4)(CO)_2(Cl)\{HB(ImMe)_3\}]$.

Keywords: organometallic compounds; tungsten; carbyne; carbene

Citation: Inglis, C.M.; Manzano, R.A.; Kirk, R.M.; Sharma, M.; Stewart, M.D.; Watson, L.J.; Hill, A.F. Poly(imidazolyliden-yl)borato Complexes of Tungsten: Mapping Steric vs. Electronic Features of *Facially* Coordinating Ligands. *Molecules* **2023**, *28*, 7761. https://doi.org/10.3390/molecules28237761

Academic Editor: Petr Kilián

Received: 10 November 2023
Revised: 21 November 2023
Accepted: 21 November 2023
Published: 24 November 2023

1. Introduction

The poly(pyrazolyl)borate class of chelates developed by Trofimenko, colloquially known as 'scorpionates' [1–3], have found broad application in diverse of areas of coordination and bioinorganic and organometallic chemistry. Key features that have contributed to their widespread deployment include (i) ease of synthesis; (ii) functionalization at both the bridgehead boron and pyrazolyl rings to provide a range of steric and electronic properties; (iii) kinetic stability of the chelated cage once coordinated to a metal centre; (iv) their so-called 'octahedral enforcer' nature, whereby the topology of the cage especially favours octahedral coordination geometries; and (v) the extension of the principle to the replacement of the pyrazol-1-yl arms with a range of other heterocycles that bridge boron and the metal to which they coordinate. Amongst these, the hydrotris(3,5-dimethylpyrazol-1-yl)borate ligand ($HB(pzMe_2)_3$, Scheme 1) has proven to be especially useful in presenting a moderate degree of steric protection to the remaining three ligands in an octahedral metal complex.

N-heterocyclic carbenes (NHC) have emerged over the last three decades, from being rather niche ligands of fundamental interest, to highly effective supporting co-ligands for the development of robust materials and, in particular, catalysts [4–6]. Fehlhammer first demonstrated the confluence of poly(azolyl)borate and NHC chemistries with reports of the first tris(*N*-alkylimidazolylidenyl)borates ($HB(ImR^1)_3$, R^1 = Me, Et, ^{i}Pr; Scheme 2) [7–10], and whilst the trimethyl derivative $HB(ImMe)_3^-$ most closely resembles the topology of the Tp* scorpionate, its chemistry has been scarcely developed beyond the original Fehlhammer work. Rather, the ligand class has been functionally elaborated to include (i) sterically imposing *N*-subtituents (R^1 = ^{t}Bu, Cy, adamantly, mesityl and 2,6-diisopropylphenyl) [11–14], (ii) macrocyclic variants [15–21], (iii) extension to bidentate examples [5,22–34], (iv) replacement of the bridgehead borohydride with phenyl or fluoro groups [35–37] and (v) substitution of the imidazolylidene bridges by triazolylidenes or benzoimidazolylidenes [35–38].

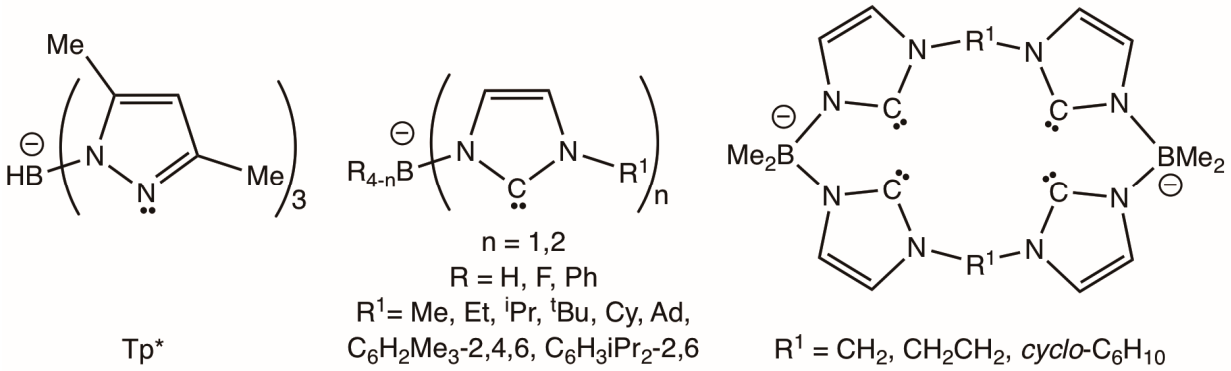

Scheme 1. Selected pyrazolyl and imidazolylidenyl borates. Tp* = hydrotris(dimethylpyrazolyl)borate.

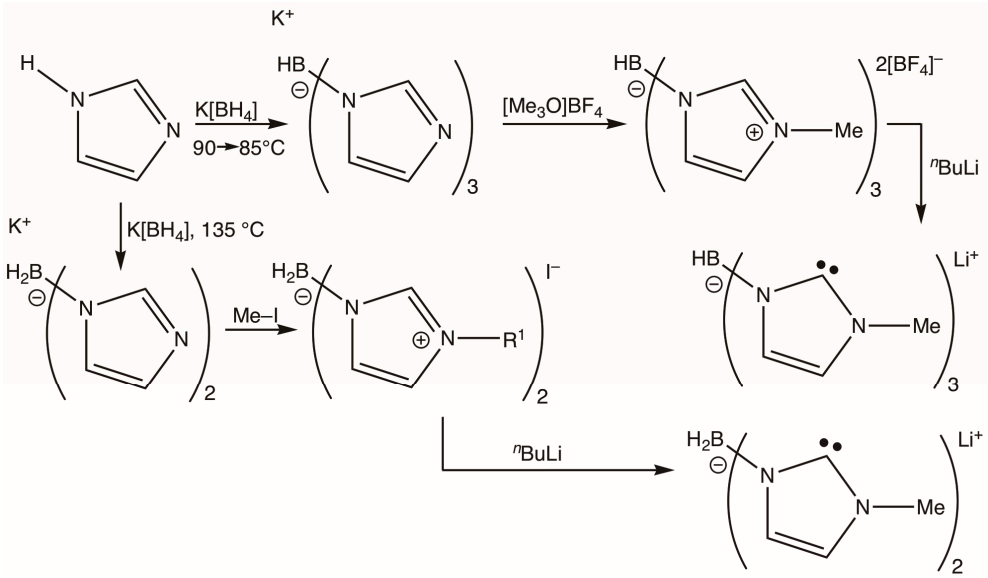

Scheme 2. Fehlhammer's syntheses of bis- and tris(*N*-methylimidazolylidenyl)borates [3].

Amongst the multitude of catalytic processes catalysed by NHC-supported mediators, the advent of Grubbs's second generation alkene metathesis catalyst and related analogues [39–42] has led to a plethora of complexes that feature both NHC and conventional alkylidene ligands. These serve to demonstrate the vastly different nature and reactivity of the metal–carbon 'multiple' bonds, whereby productive metathesis involves the alkylidene ligand exclusively, while the NHC ligand remains innocent. That said, an early report by Lappert described the metathesis of electron-rich alkenes by an NHC complex devoid of alkylidene ligands [43]. In contrast, alkylidyne complexes with metal–carbon triple bonds that are supported by NHC ligands are somewhat scarcer [44–57] with most examples having emerged from the groups of Esteruelas and Buchmeiser. The intersection of poly(imidazolylidenyl)borates with the chemistry of metal–carbon multiple bonds would appear limited to a single macrocyclic complex [Fe(=CPh_2)({$Me_2B(C_3N_2H_2)_2C_6H_{10}$}$_2$)] [21]. Given the important role that poly(pyrazolyl)borate ligands have played in the development of alkylidyne chemistry [58], herein we report the first carbyne complex ligated by a poly(imidazolylidenyl)borate, [W(≡CC_6H_4Me-4)$(CO)_2${$HB(ImMe)_3$}] ($HB(ImMe)_3$ = hydrotris(3-methylimidazoylyliden-1-yl)borate) which provides an opportunity to benchmark the donor properties of the $HB(ImMe)_3$ ligand against more familiar tripodal tridentate ligands. The complex also serves as a precursor to the first heterometallic complex of a poly(imidazolylidenyl)borate viz. [WAu(μ-CC_6H_4Me-4)$Cl(CO)_2${$HB(ImMe)_3$}].

2. Results

2.1. Pro-Ligand Synthesis

Fehlhammer's original synthetic approach (Scheme 2) [7] involved threefold alkylation of potassium hydrotris(imidazol-1-yl)borate with Meerwein's salt $[Me_3O]BF_4$, this latter reagent being the most expensive component. Apart from blazing the original trail, Fehlhammer's approach allows for the installation of various carbene alkyl *N*-substituents at a late stage on a common late synthetic intermediate.

We have developed an alternative synthesis that borrows from protocols developed for more sterically encumbered examples described by Smith [11–14]. Whilst demonstrating no new principles here, our approach does offer both convenience and economy, employing cheap commercially available reagents (Scheme 3).

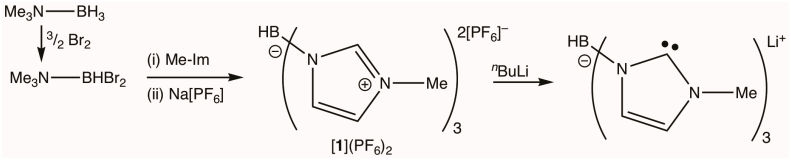

Scheme 3. Alternative syntheses of tris(*N*-methylimidazolylidenyl)borate salts.

The reaction of $[Me_3N{\cdot}BH_3]$ with bromine affords $[Me_3N{\cdot}BHBr_2]$ [59], which may be generated in situ without isolation. Subsequent treatment with *N*-methylimidazole affords the salt $[HB(ImMeH)_3]Br_2$ ($[1]Br_2$). This salt, whilst forming in high yields, is difficult to manipulate as it is exceedingly deliquescent and upon filtration under ambient air rapidly forms a sticky syrup. This behaviour is potentially problematic since the subsequent step calls for deprotonation via strong, moisture-sensitive bases, e.g., ^{n}BuLi or $KN(SiMe_3)_2$. Metathesis with aqueous $Na[PF_6]$, however, results in ready recovery of the hexafluorophosphate salt $[HB(ImMeH)_3](PF_6)_2$ ($[1](PF_6)_2$), which is not hygroscopic and crystallizes free of water as confirmed via a crystallographic analysis (Figure 1).

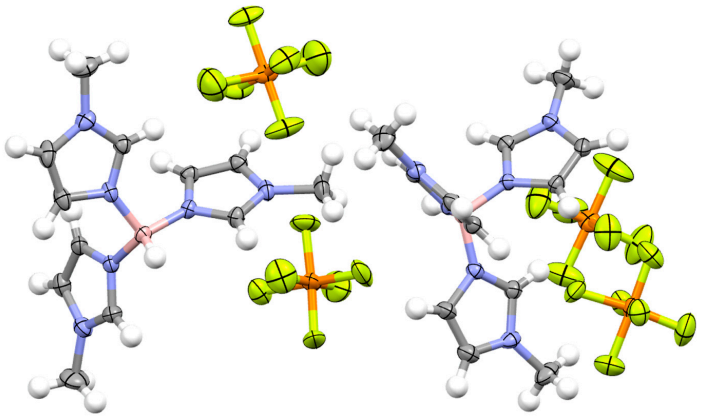

Figure 1. Structure of the hydrotris(*N*-methylimidazolyl)boronium salt $[HB(ImMeH)_3](PF_6)_2$ ($[1](PF_6)_2$ (two crystallographically independent molecules shown, 50% displacement ellipsoids, major occupancies of positionally disordered PF_6 anions shown).

2.2. Ligand Installation

For installation of the pro-ligand on a suitable alkylidyne precursor, the 4-toluidyne complex *trans*,*cis*,*cis*-$[W(\equiv CC_6H_4Me\text{-}4)(CO)_2(pic)_2Br]$ (pic = 4-picoline) (**2a**) was chosen to exploit the lability of the bromide and 4-picoline ligands. Whilst this complex has not been previously reported on, its synthesis (Scheme 4) is unremarkable and mirrors that of the known xylyl or mesityl analogues [60–62]. Synthetic procedures are presented alongside those for the molybdenum analogue (**2b**) in the Experimental section in addition to a crystallographic analysis.

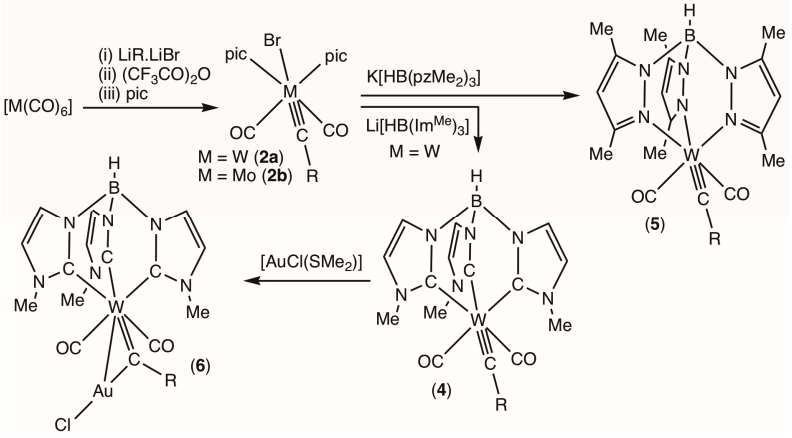

Scheme 4. Synthesis of mono- and bi-metallic toluidyne complexes ligated by the $HB(Im^{Me})_3$ ligand (R = C_6H_4Me-4, pic = 4-picoline = NC_6H_4Me-4).

The pro-ligand salt [1] $(PF_6)_2$ was dissolved in tetrahydrofuran and cooled (dry ice/propanone) before addition of 3 equivalents of ^{n}BuLi, followed by slow warming to room temperature to provide a yellow solution of Li[HB(ImMe)$_3$] (Li [3]) which was re-cooled and treated with **2a**. Re-warming to room temperature resulted in a colour change to dark brown as the infrared absorptions for the starting material (**2a**: ν_{CO} = 1986, 1898) were replaced with those of the new product (**4**: ν_{CO} = 1958, 1873 cm^{-1}). After stirring for 3 h, the product was isolated via column chromatography to yield a bright orange microcrystalline powder.

Spectroscopic data were consistent with the formulation of the desired product [W(≡CC_6H_4Me-4)(CO)$_2${HB(ImMe)$_3$}] (**4**). Amongst these, the most conspicuous datum is that for the carbyne resonance in the $^{13}C\{^1H\}$ NMR spectrum (CD_2Cl_2: δ_C = 280.7, $^1J_{WC}$ = 171.4 Hz). Consistent with the inferred C_s symmetry of the molecule, the carbonyls gave rise to a single resonance (δ_C = 223.3, $^1J_{WC}$ = 132.0 Hz) while the tungsten-bound carbon nuclei of the NHC donors gave rise to two resonances at a ratio of 2:1 with markedly different chemical shifts and $^1J_{WC}$ couplings ($\delta_C/^1J_{WC}$ = 192.0/95.2), 181.3/44.7). With the exception of the complexes [Pt{$H_2B(ImR^1)_2$}$_2$] (R^1 = Me, Et) for which $^1J_{PtC}$ values were not reported [8], and [Rh(CO)(L){$X_2B(ImR)_2$] (L = CO, PPh_3, PCy_3; X = H, F; R = Ph, Cy) [31], poly(imidazolylidenyl)borates have not previously been coordinated to metal nuclei with usefully spin-active ($I = \frac{1}{2}$) isotopes.

As **4** is the first tungsten complex of such a ligand, it provides an opportunity to demonstrate the special feature of $HB(ImR^1)_3$ chelates cf. poly(pyrazolyl)borates; scalar couplings observed in the $^{13}C\{^1H\}$ NMR spectra may serve as reporters to interrogate metal–carbon bonding. Thus, whilst the chemical shift and associated coupling for the carbon nuclei trans to the carbonyl ligands are unremarkable (e.g., cf. the conventional NHC complex [W{=C(ND^{i}PP)$_2$C$_2$H$_2$}(CO)$_5$]: δ_C = 187.9, $^1J_{WC}$ = 105.7 Hz, DiPP = $C_6H_3{}^iPr_2$-2,6) [63], the resonance for the carbon trans to the carbyne is shifted some 11 ppm to higher field and displays a dramatically reduced coupling to tungsten-183 (44.7 Hz). These may be taken as indicating a weaker W–C interaction which in turn reflects the pronounced trans influence of the alkylidyne ligand, a feature well-documented in the structural chemistry of alkylidyne complexes ligated via poly(pyrazolyl)borate ligands [58]. As to the impact of the $HB(ImMe)_3$ ligand on the remaining co-ligands, comparison with the known complex [W(≡CC_6H_4Me-4)(CO)$_2$(Tp*)](**5**) [64] (Tp* = hydrotris(dimethylpyrazoyl)borate, prepared here from K[Tp*] and **2a**, see Experimental) is useful. The carbyne and carbonyl resonances for the Tp* derivative appeared at almost identical frequencies to those of the $HB(ImMe)_3$ complex [$\delta_C(^1J_{WC}$/Hz) = 279.2 (186.6), 224.0 (166.2)]; however, in both cases, the magnitudes of $^1J_{WC}$ values were significantly larger for **5** than for **4**. Insofar as these may be taken as being indicative of the strength of the metal–carbon interaction, it would appear that the NHC donors weaken both the carbyne and carbonyl binding. This is, however, difficult to

reconcile with the ν_{CO}-associated infrared data which comprise A_1 and B_1 modes observed at 1958 and 1873 cm^{-1} in dichloromethane (ATR: 1949, 1867 cm^{-1}). These are amongst the lowest observed for neutral complexes of the form [W(≡CC_6H_4Me-4)$(CO)_2$(L)] where L is one of a range of nominally tripodal facially capping ligands [58,64–67]. These values are even lower than for the π-donor ligand $HB(mt)_3$ (1967, 1875 cm^{-1}; mt = 2-mercapto-*N*-methyl-imidazol-1-yl) [67] and Kläui's (η^5-C_5H_5)$Co(PO_3Me_2)_3$ ligand [68]. It would therefore appear that the $HB(ImMe)_3$ ligand makes the tungsten centre especially electron rich and this may be verified using cyclic voltammetry (Figure 2). For both **4** and **5**, sweeping the voltage to *ca* +2 V reveals two oxidation processes, neither of which appear reversible. Limiting the sweep to *ca* 1.0 V indicates that the reversibility of first oxidation event increases with increasing sweep rate. For **5**, ΔE_p increases slightly with increased scan rate from 0.180 (0.1 Vs^{-1}) to 0.250 V (0.3 Vs^{-1}) suggesting the oxidation is essentially reversible with $E_{\frac{1}{2}}$ = 0.34 V ($E_{p,c}$ = 0.43 at 0.1 Vs^{-1}). For **4** the dependence of ΔE_p on sweep rate is more significant, increasing from 0.170 V at 0.1 Vs^{-1} ($E_{p,c}$ = 0.33 V) to 0.630 V at 5 Vs^{-1}($E_{p,c}$ = 0.64 V) is observed. Thus, fast sweep rates are required to observe a reasonable degree of reversibility, with, however, an almost identical half-wave potential ($E_{\frac{1}{2}}$ 0.345 V) to that of **5**. Chemical oxidation of tris(pyrazolyl)borate carbyne complexes of tungsten is typically accompanied by decarbonylation [65,69–71], which most likely accounts for the poor reversibility at slow sweep rates or higher voltages.

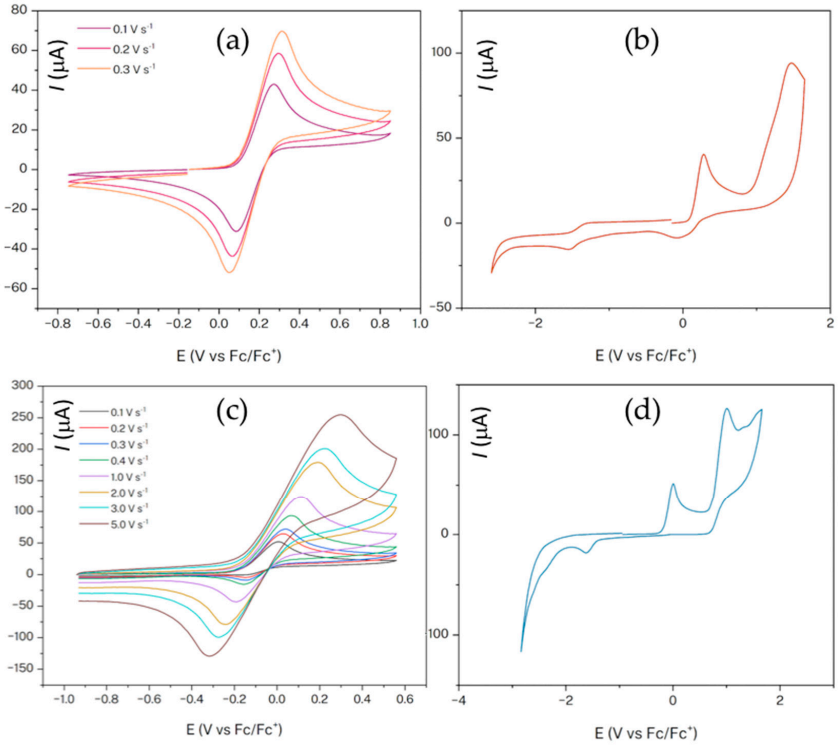

Figure 2. Cyclic voltammetry of [W(≡CC_6H_4Me-4)$(CO)_2$(L)] (L = $HB(pzMe_2)_3$ **5**, $HB(ImMe)_3$ **4**) (Silver wire *pseudo*-reference electrode, anaerobic 1 mM in CH_2Cl_2, 0.1 M [NBu_4][PF_6] supporting electrolyte; ferrocene reference $E_{1/2}$ = 0.460 V cf. Ag/Ag^+ = 0). (**a**) Reversibility CV at varied scan rates of **5** (0 V → +1.0 V → –0.6 V). (**b**) Full window CV of **5** (0 V → +1.8 V → –2.5 V, υ = 0.1 Vs^{-1}). (**c**) Reversibility CV at varied scan rates of **4** (0 V → +0.9 V → –0.6 V). (**d**) Full window CV of **4** (0.6 V → +2.0 V → –2.5 V, υ = 0.1 Vs^{-1}).

2.3. Quantification of Steric and Electronic Features

A popular and time-honoured method for assessing the donor properties of ligands involves their impact on infrared frequencies of carbonyl co-ligands. This is traditionally assayed, in the case of phosphines, using the Tolman electronic parameter ν^T, viz. the fre-

quency of the A_1 mode of CO vibrations in a host of complexes of the form [Ni(L)$(CO)_3$] [72]. Although similar scales may be developed for NHC ligands coordinated to the 'Ni$(CO)_3$' fragment [73–75], the toxicity of nickel carbonyl has led to the advent of alternative scales based on the RhCl$(CO)_2$ fragment (average of A_1 and B_1 modes) as the preferred platform, alongside metrics derived from NMR data for the NHC bound to selenium (=Se, δ_{Se}), phenylphosphinidine (=PPh, δ_P) or $PdBr_2\{C(N^iPr)_2C_6H_4\}$ (δ_C) fragments [76]. These methods are not directly applicable to $H_nB(ImR^1)_{4-n}$ complexes due to their negative charge and chelation. While it would be reasonable to presume that, as with conventional neutral NHC ligands, these will be potent net donors, it would be useful to be able to benchmark both the electronic and steric features of poly(imidazolylidenyl)borate ligands against those of more familiar facially capping nominally tridentate (κ^3, η^5 or η^6) ligands, of which there are many. Smith has already suggested such a ranking for a small number of facial/tripodal ligands based on the ν_{NO} stretching frequencies of complexes of the form [Ni(NO)(L)] [37]. Such ligands may be grouped according to their charge (neutral, mono- or di-anionic) which in turn impacts the charge of the derived complexes (cationic, neutral or anionic, respectively). In the case of complexes of the form $[W(\equiv CC_6H_4Me\text{-}4)(CO)_2(L)]^{x+}$, a number of these have been compared in terms of the experimentally determined infrared data for the cis-dicarbonyl oscillator [67,77–89]. In addition to the frequencies of the observed symmetric and antisymmetric modes (A_1 $\nu_{s(CO)}$, B_1 $\nu_{as(CO)}$), the two numbers may be condensed into a singular Cotton–Kraihanzel force constant [90]. This is reasonable in the case of $[W(\equiv CR)(CO)_2(L)]^{x+}$ because the two carbonyl ligands are chemically equivalent, i.e., both individual CO oscillators are identical. This is perhaps less appropriate in the 'RhCl$(CO)_2$' system, where in any event the simple arithmetic mean is usually employed.

Our previous collation was based on experimentally determined ν_{CO} values with the caveat that some were acquired from solid-state mesurements (Nujol mulls, KBr discs, ATR, etc.) while others were obtained from a variety of solvents. Infrared data for metal carbonyls are prone to significant perturbation in the solid state due to different crystal modifications or crystallographically independent molecules within the same crystal which in each case place the CO ligand(s) in different environments. The solvent-dependent nature of IR data for metal carbonyls, due to which both the frequency and broadening are significantly impacted by the choice of solvent, has long been recognized [91]. Thus, gas phase data, when measurement is viable, typically produce higher frequencies than are found in aliphatic hydrocarbons, and while such solvents provide the sharpest and therefore best-resolved peaks, comparatively few carbonyl complexes are sufficiently soluble. Dichloromethane has therefore become the solvent of choice offering the most accommodating solubility characteristics and reasonably narrow peaks.

To obviate these imponderables, we have collated infrared data for a range of complexes $[W(\equiv CC_6H_4Me\text{-}4)(CO)_2(L)]^{x+}$ derived from computational interrogation (Table 1). Our intention is *not* to provide the most precise current state-of-the-art investigation of the intimate bonding and thermodynamic properties of such complexes but rather to derive a readily accessible and computationally economic comparative scale. A useful corollary of this approach is that the optimised geometries used for frequency calculations may be employed to directly calculate the percentage buried volume (%V_{bur}) [92,93] of each ligand L. The %V_{bur} approach to quantifying the steric impact of a ligand is especially suitable for ligands with irregular topologies, and for phosphines, such analysis reassuringly returns a correlation approximately linear with Tolman's cone angle (θ^T = 3.95x%V_{bur} + 31.5) [94]. Accordingly, a scatter plot of the Cotton–Kraihanzel force constant k_{CO} vs. %V_{bur} (Figure 3) may be presented for ligands L that is reminiscent of the familiar ν^T vs. θ^T plot used to map phosphine electronic and steric space [72]. For this purpose, with this combination of density functional, basis set and anharmonic scaling factor the value of the Cotton–Kraihanzel force constant reduces to the following equation:

$$k_{CO}\ [Ncm^{-1}] = 1.7426 \times 10^{-6}\ Ncm \times (\nu_s{}^2 + \nu_{as}{}^2)$$

Table 1. Experimental [a] and calculated [b] infra-red and steric [c] properties of $[W(\equiv CC_6H_4Me)(CO)_2(L)]^{x+}$.

	L	x	$\nu_{(CO)}$/cm^{-1} Experimental [a]	k_{CK}/Ncm^{-1} [d]	$\nu_{(CO)}$/cm^{-1} Calculated [b]	k_{CK}/Ncm^{-1} $\lambda_1(\lambda_2)$ [i]	$\nu_{(WC)}$/cm^{-1}	%Vol$_{bur}$ [c]	Ref
1	**κ^3-HB(ImMe)$_3$**	**0**	**1958, 1873**	**14.80**	**1969, 1907**	**15.15 (14.76)**	**1334**	**52.4**	**-**
2	**κ^3-HB(pzMe$_2$)$_3$** [g]	**0**	**1971, 1889** [c]	**15.07**	**1980, 1912**	**15.27 (14.86)**	**1350**	**50.7**	[64]
3	η^5-$C_2B_9H_9Me_2$	1–	1956, 1874	14.82	1970, 1900	15.10 (14.71)	1354	49.6	[79]
4	κ^3-CpCo(PO$_3$Me$_2$)$_3$	0	1961, 1859	14.74	1980, 1906	15.23 (14.83)	1353	44.0	[68]
5	κ^3-HB(mt)$_3$	0	1967, 1875	14.91	1983, 1916	15.33 (14.93)	1352	48.7	[67]
6	η^5-$C_2B_9H_{11}$	1–	1965, 1880	14.93	1974, 1906	15.18 (14.77)	1356	44.3	[79]
7	κ^3-Me3[9]aneN$_3$ [e]	1+	1975, 1879 [f]	15.00	2003, 1940	15.68 (15.27)	1347	52.5	[80]
8	κ^3-HC(py)$_3$ [e]	1+	1988, 1894 [b,f]	15.22	2007, 1949	15.78 (15.37)	1346	46.2	[81]
9	κ^3-[9]aneS3 [e,h]	1+	2007, 1925 [f]	15.59	2029, 1980	16.20 (15.78)	1346	46.0	[81]
10	η^5-C_5H_5	0	1982, 1902	15.24	1997, 1941	15.64 (15.23)	1348	35.2	[82]
11	κ^3-HB(pz)$_3$ [k]	0	1986, 1903	15.28	1998, 1934	15.49 (15.11)	1347	43.3	[84]
12	η^5-C_5Me_5	0	1981, 1910 [c,j]	15.29	1989, 1933	15.51 (15.12)	1349	42.4	[86]
13	κ^3-HC(pz)$_3$	1+	1995, 1912	15.42	2016, 1959	15.93 (15.52)	1347	41.7	[87]
14	η^6-$C_2B_{10}H_{10}Me_2$	1–	1990, 1930	15.52	1981, 1932	15.44 (15.04)	1352	53.5	[89]
15	κ^3-P(py)$_3$ [e]	1+	2007, 1925 [f]	15.62	2008, 1951	15.80 (15.39)	1349	47.9	[81]
16	κ^3-MeC(CH$_2$Ph$_2$)$_3$ [e,g]	1+	1999, 1934 [b,f]	15.62	*2095, 2037*	*17.01 (15.46)*	*n.r.*	*59.8*	[81]
17	κ^3-HC(pzMe$_2$)$_3$	1+	–	–	2002, 1941	15.68 (15.27)	1349	49.1	–
18	κ^3-MeC(CH$_2$Pme$_2$)$_3$	1+	–	–	2021, 1974	16.09 (15.67)	1342	51.5	–
19	η^6-C_6H_6	1+	–	–	2051, 2017	16.68 (16.25)	1356	39.3	–
20	η^6-C_6Me_6	1+	–	–	2030, 1989	16.28 (15.85)	1351	45.9	–
21	η^6-C_6Et_6	1+	–	–	2019, 1975	16.08 (15.66)	1351	53.3	
22	η^5-C_9H_7 (indenyl)	0	–	[h]	2002, 1949	15.74 (15.32)	1348	37.3	[61]
23	η^5-$C_{13}H_9$ (fluorenyl)	0	–	–	1999, 1941	15.65 (15.24)	1356	40.4	–
24	η^5-C_5Ph_5 [g]	0	–	–	*2077, 2015*	*16.88 (15.34)*	*1532*	*48.3*	–
25	η^5-C_5Cl_5	0	–	–	2012, 1962	15.92 (15.51)	1354	40.8	–
26	η^5-$C_5H_3(SiMe_3)_2$-1,3	0	–	–	1987, 1931	15.48 (15.08)	1307	54.5	–
27	η^5-C_5Me_4N	0	–	–	1992, 1937	15.56 (15.16)	1350	39.2	–
28	η^5-C_5Me_4P	0	–	–	1990, 1937	15.55 (15.15)	1348	41.7	–
29	η^5-C_5Me_4As	0	–	–	1989, 1936	15.53 (15.13)	1348	37.5	–
30	η^5-C_5H_5BH	0	–	–	2006, 1953	15.80 (15.39)	1351	40.8	–
31	κ^3-MeB(CH$_2$PPh$_2$)$_3$ [g]	0	–	–	*2072, 2003*	*16.74 (15.22)*	*1519*	*59.8*	–
32	κ^3-MeB(CH$_2$Pme$_2$)$_3$	0	–	–	1988, 1933	15.50 (15.10)	1339	51.2	–
33	κ^3-MeB(CH$_2$Sme)$_3$	0	–	–	1996, 1935	15.58 (15.17)	1348	49.7	–
34	κ^3-HB(mt^{Se})$_3$	0	–	–	1981, 1915	15.31 (14.91)	1357	49.7	–
35	κ^3-HB(ImEt)$_3$	0	–	–	1968, 1906	15.13 (14.74)	1322	54.4	–
36	κ^3-HB(Im^{i}Pr)$_3$	0	–	–	1970, 1907	15.16 (14.76)	1340	53.1	
37	κ^3-HB(Im^{t}Bu)$_3$	0	–	–	1950, 1881	14.80 (14.41)	1334	59.5	–
38	κ^3-HB(ImPh)$_3$	0	–	–	1981, 1919	15.34 (14.94)	1329	54.3	–
39	κ^3-HB(ImCF$_3$)$_3$	0	–	–	1999, 1947	15.70 (15.29)	1337	57.1	

[a] Unless otherwise indicated, data were determined from dichloromethane solutions. [b] DFT:ωB97X-D/6-31G*/LANL2Dζ(W)/Gas-phase, anharmonic scaling factor 0.9420. [c] Percentage buried volume calculated [92] for a 3.5 Å sphere centred on tungsten with H-atoms included. [d] Cotton–Kraihanzel force constant [90]. [e] Experimental data for benzylidyne. [f] KBr pellet. [g] Values in italics were determined at the reduced PM3tm level of theory. [h] $[Mo(\equiv CC_6H_3Me_2$-2,6$)(CO)_2(\eta^5$-$C_9H_7)]$ has ν_{CO} = 1998, 1925 cm^{-1} [61]. [i] λ_1 = 0.9420, λ_2 = 0.9297. [j] Measured in *n*-hexane. [k] The complex $[W(\equiv CC_6H_4Me$-4$)(CO)_2\{B(pz)_4\}]$ has identical ν_{CO} values to those for $[W(\equiv CC_6H_4Me$-4$)(CO)_2\{HB(pz)_3\}]$, i.e., replacing the remote B–H substituent with pz has negligible electronic impact. *n.r.* = not identified with confidence or heavily coupled with other oscillators.

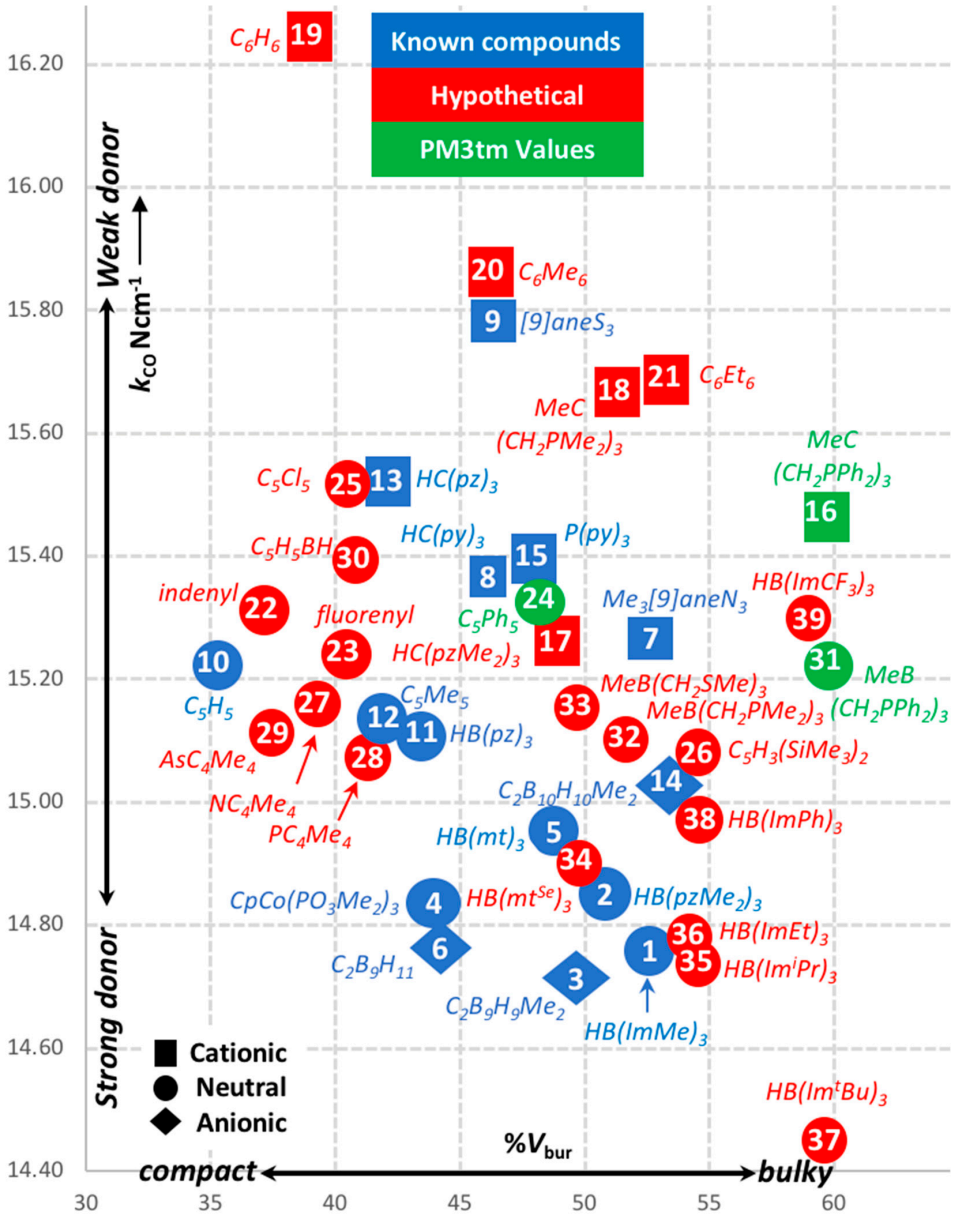

Figure 3. Electronic (k_{CO}) vs. steric (%V_{bur}) map for a range of facially coordinating ligands derived computationally (DFT:ωB97X-D/LANL2Dζ(W)). A small number (shown in green) were calculated at the semi-empirical PM3tm level of theory due to their large atom count, for which the ordinate positions should be treated with appropriate reservation.

The ωB97X-D [95,96] functional was employed with the 6-31G* basis set [97] in combination with the LANL2Dζ effective core potential for tungsten [98–100], and while much more sophisticated levels of theory are certainly available, this selection represents a balance between utility and computational economy for these medium-sized molecules. For larger ligands 'L', where steric bulk has or might be an intentional design feature, %V_{bur} values obtained at the simpler semi-empirical PM3tm level of theory are used, as we are here only concerned with molecular topologies (Figure 4). Taking complexes of the ligands HB(pzMe$_2$)$_3$, HB(ImMe)$_3$ and MeC(CH$_2$PMe$_2$)$_3$ as test cases, the variation in %V_{bur} calculated between ωB97X-D/6-31G*/LANL2Dζ and PM3tm methods was <3%, i.e., within the magnitude of molecular libration. Vibrational frequencies, whilst calculated to ensure local minima had been located, were imprecise at the PM3tm level and considered of little use. Accordingly, the ordinate location of such ligands in Figure 3 (shown in green) should be viewed with considerable caution. These were derived with little rigour by simply

scaling the PM3tm k_{CO} values by 0.9089, this being the ratio of k_{CO} values calculated at the PM3tm and DFT levels of theory for **4** and **5**. That said, the peripheral inclusion of sterically obtrusive substituents in ligands often results in rather limited transmission of inductive electronic effects to the metal centre itself, as seen, for example, in experimental data for L = η^5-C_5H_5 (k_{CO} = 15.24 Nm^{-1}) and η^5-C_5Me_5 (k_{CO} = 15.29 Nm^{-1}). Similarly, experimental data are not available for toluidyne complexes of all ligands L, in which cases experimental data for the corresponding phenyl or xylyl carbynes are instead provided alongside those calculated for the toluidyne.

Table 2. Calculated (TT-DFT) [a] electronic absorptions of interest, natural atomic charges (*Z*) and Löwdin bond orders (LBO) for selected complexes $[W(\equiv CC_6H_4Me)(CO)_2(L)]^{x+}$.

	L	x	λ_{max}/nm $d_{xy}\rightarrow\pi^*_{W\equiv C}$	λ_{max}/nm $\pi_{W\equiv C}\rightarrow\pi^*_{W\equiv C}$	*Z*(W)	*Z*(C)	LBO (W≡C)	*r*(W≡C)/Å
1	**κ^3-HB(ImMe)$_3$ (4)**	**0**	**433**	**332**	**+0.748**	**−0.316**	**2.37**	**1.833**
2	**κ^3-HB(pzMe$_2$)$_3$ (5)**	**0**	**406**	**316**	**+1.013**	**−0.268**	**2.40**	**1.811**
3	η^5-$C_2B_9H_9Me_2$	1−	435	359	+0.831	−0.214	2.35	1.810
4	κ^3-CpCo(PO_3Me_2)$_3$	0	431	374	+1.177	−0.299	2.40	1.802
5	κ^3-HB(mt)$_3$	0	444	335	+0.685	−0.256	2.42	1.800
6	η^5-$C_2B_9H_{11}$	1−	428	358	+0.845	−0.230	2.36	1.810
7	κ^3-Me_3[9]aneN$_3$ [b]	1+	400	377	+0.858	−0.188	2.39	1.812
8	κ^3-HC(py)$_3$ [x]	1+	403 [b]	377 [b]	+0.909	−0.213	2.40	1.813
9	κ^3-[9]aneS$_3$	1+	377	330	+0.405	−0.131	2.35	1.818
10	η^5-C_5H_5	0	420	319	+0.851	−0.270	2.40	1.815
11	κ^3-HB(pz)$_3$	0	412	313	+0.979	−0.253	2.42	1.810
12	η^5-C_5Me_5	0	430	326	+0.870	−0.284	2.41	1.814
13	κ^3-HC(pz)$_3$ [b]	1+	405	337	+0.886	−0.190	2.41	1.811
14	η^6-$C_2B_{10}H_{10}Me_2$	1−	417	372	+0.732	−0.171	2.34	1.811
15	κ^3-P(py)$_3$ [b]	1+	384	332	+0.911	−0.214	2.40	1.809
17	κ^3-HC(pzMe$_2$)$_3$	1+	386	319	+0.920	−0.208	2.40	1.810
18	κ^3-MeC(cH_2PMe_2)$_3$	1+	390	335	+0.146	−0.130	2.33	1.830
19	η^6-C_6H_6	1+	356	381	+0.697	−0.105	2.32	1.820
20	η^6-C_6Me_6	1+	386	333	+0.754	−0.134	2.35	1.813
21	η^6-C_6Et_6	1+	379	336	+0.759	−0.130	2.33	1.814
22	η^5-C_9H_7 (indenyl)	0	415	354	+0.889	−0.269	2.45	1.802
23	η^5-$C_{13}H_9$ (fluorenyl)	0	436	357	+0.909	−0.237	2.45	1.798
25	η^5-C_5Cl_5	0	422	323	+0.851	−0.214	2.41	1.805
26	η^5-$C_5H_3(SiMe_3)_2$-1,3	0	418	318	+0.849	−0.257	2.40	1.812
27	η^5-C_4Me_4N	0	415	326	+0.939	−0.273	2.40	1.811
28	η^5-C_4Me_4P	0	391	365	+0.755	−0.247	2.37	1.816
29	η^5-C_4Me_4As	0	390	366	+0.740	−0.255	2.37	1.816
30	η^5-C_5H_4BH	0	383	323	+0.769	−0.164	2.37	1.811
32	κ^3-MeB(cH_2PMe_2)$_3$	0	412	329	+0.274	−0.213	2.37	1.825
33	κ^3-MeB(cH_2SMe)$_3$	0	422	323	+0.587	−0.224	2.40	1.809
34	κ^3-HB(mt^{Se})$_3$	0	443	338	+0.631	−0.263	2.42	1.800
35	κ^3-HB(ImEt)$_3$	0	424	329	+0.763	−0.324	2.35	1.835
36	κ^3-HB(Im^{i}Pr)$_3$	0	437	335	+0.749	−0.318	2.38	1.830
37	κ^3-HB(Im^{t}Bu)$_3$	0	423	322	+0.864	−0.294	2.33	1.820
38	κ^3-HB(ImPh)$_3$	0	449	335	+0.960	−0.300	2.37	1.828
39	κ^3-HB($ImCF_3$)$_3$	0	426	329	+0.689	−0.238	2.37	1.824

[a] TD-DFT:ωB97X-D/6-31G*/LANL2Dζ(W)/gas-phase. [b] $\pi^*_{W\equiv C}$ does not correspond to the LUMO due to low-lying ligand(L)-centred virtual orbitals.

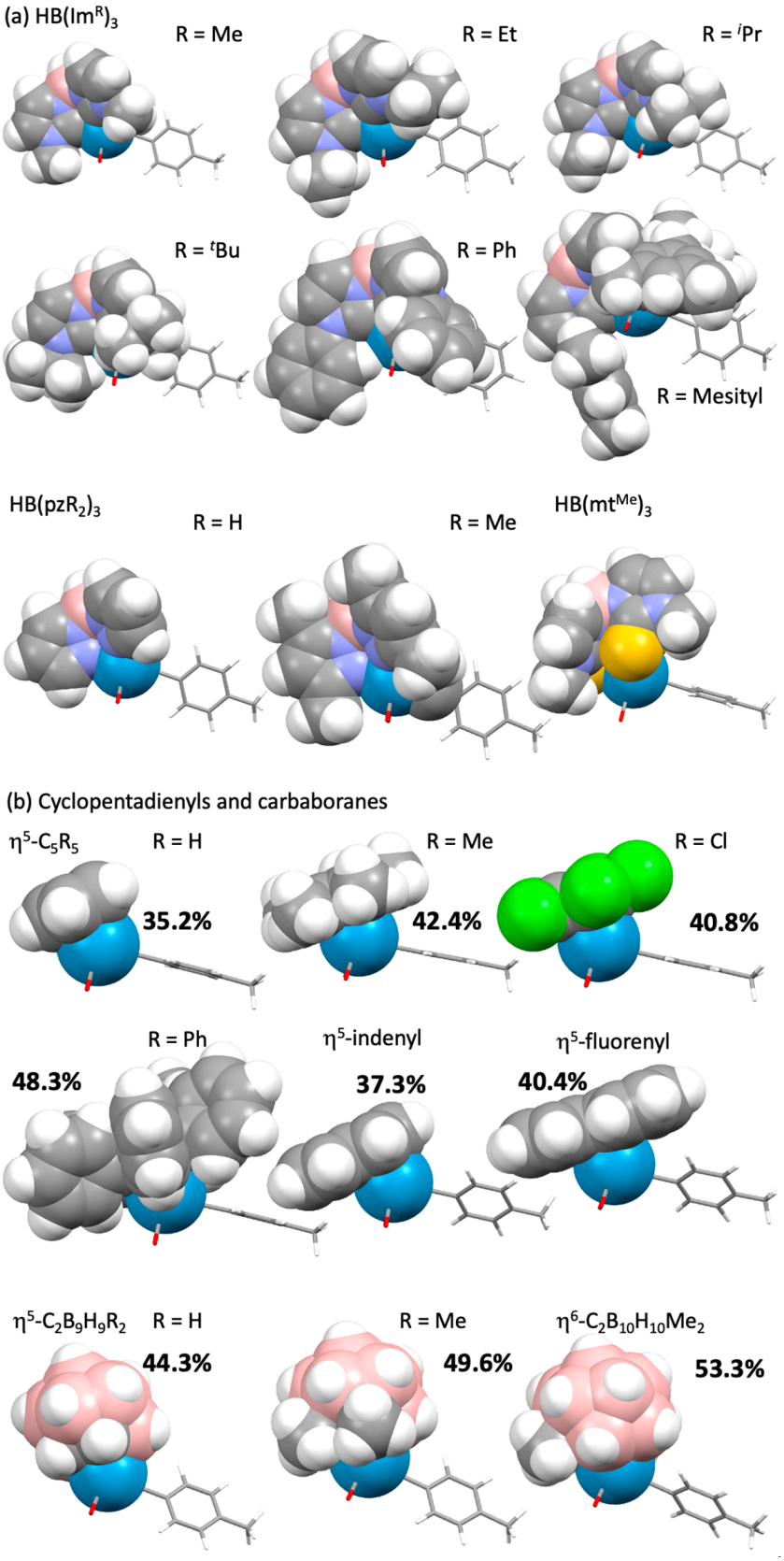

Figure 4. *Cont.*

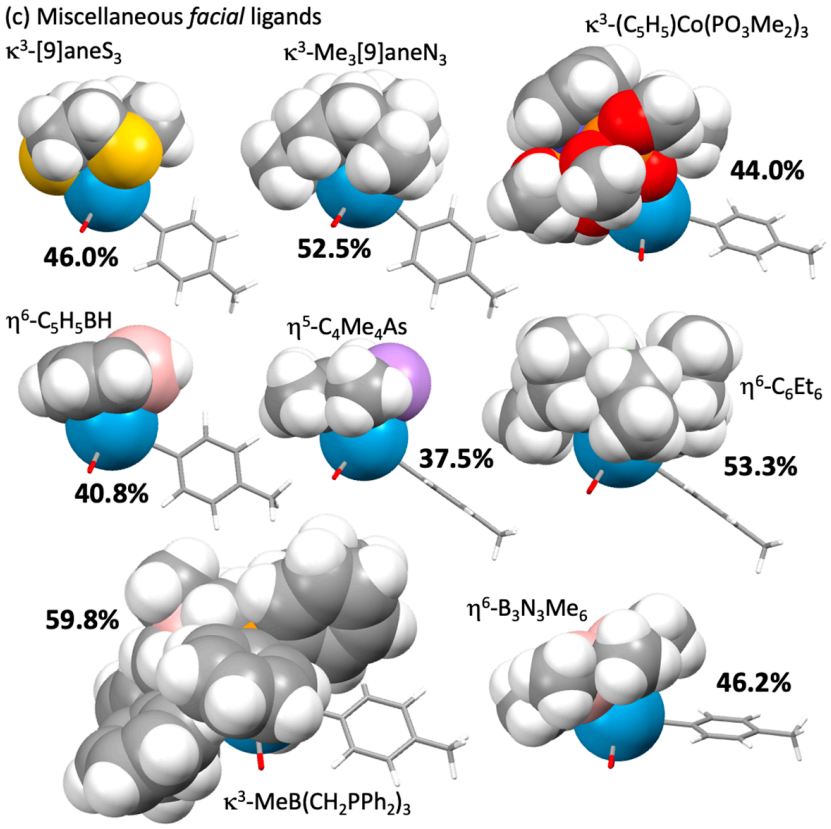

Figure 4. Corey–Pauling–Koltun representations of facial ligand from Tables 1 and 2 in the complexes [W(≡CC_6H_4Me-4)$(CO)_2$(L)] toluidyne and carbonyl ligands simplified). (**a**) Poly(azolyl)borates; (**b**) cyclopentadienyls and carbaboranes; (**c**) miscellaneous facial ligands.

A bonus of the requisite frequency calculations is that the vibrational mode for the W≡C bond may be readily identified, though in contrast to similar essentially 'pure' vibrations for terminal oxo (M≡O) and toluidyne (M≡N) ligands, this is by necessity coupled to the vibration of the C–C bond connecting it to the aryl substituent. This mode appears within a remarkably narrow frequency range (1345–1356 cm^{-1}), with the exception of **4** (1334 cm^{-1}), perhaps also reflecting the electron-releasing nature of the $HB(ImMe)_3$ ligand. The intensity of this mode, however, varies substantially, such that in some cases it is unlikely to be unambiguously identified in experimental IR spectra. This invariance in the value of ν_{WC} is also reflected in the derived Löwden bond orders (Table 2) for this bond, which fall within the very narrow range of 2.32–2.41. This is despite considerable variation in the calculated natural charge on tungsten (+0.405 to +1.177), while that for carbon is *comparatively* invariant (–0.105 to –0.299); i.e., electroneutrality would appear to balance charge distribution within the 'LW' unit so as to not significantly transmit this influence to the carbyne ligand.

Table 1 presents ν_{CO} frequencies corrected by an anharmonic scaling factor (λ_1) of 0.9740 as implemented in the *SPARTAN20*® software for the ωB97X-D/6-31G* combination [101,102], which, however, still overestimates these frequencies relative to those observed experimentally. Calculated vibrational frequencies generally exceed experimentally determined values due to incomplete incorporation of electron correlation, neglect of mechanical anharmonicity and the use of finite basis sets [103–105].

This overestimation is assumed to be relatively uniform, allowing for the development of generic scaling factors (λ) derived via least-squares analysis of calculated vs. experimental frequencies for various test sets of molecules. Such test sets typically involve small molecules comprising first and second row elements but rarely metals. Moreover, single scaling factors are not universally appropriate for the entire vibrational spectroscopy

range (400–4000 cm^{-1}) [106], and the fundamental modes from which they are derived generally fall below the range of interest to organometallic chemists (1800–2200 cm^{-1}). For the present discussion, it therefore seems appropriate to consider an alternative scaling factor (λ_2 = 0.9297), which we have derived from consideration of 18 experimental and fundamental modes from Table 2, with the caveat that only data measured in dichloromethane solutions were used, discarding those from solid-state or alkane solution measurements. Gas phase data were calculated, since there seemed little benefit in introducing further artificial approximations such as conductor-like polarizable continuum, molecular electron density (SMD) or conductor-like screening models (COSMO) [107–111] when the aim was to construct an approximate but internally consistent steric–electronic map rather than to seek out absolute values.

The data points may be loosely grouped according to the charge on the complex, with the general observation that as this increased from anionic through neutral to cationic, so too did the k_{CO} value. It should, however, be noted that these groupings are not well separated. Rather, some cationic complexes are coordinated by strong net σ-donors, e.g., *N*,*N*′,*N*″-trimethyltriazacyclononane (Me_3[9]aneN_3, Entry **7**) and tris(dimethylpyrazolyl)methane ($HC(pzMe_2)_3$, Entry **17**), such that comparatively low values are observed for ν_{CO} and k_{CO}. Likewise, the icosohedral dicarbollide complexes $[W(\equiv CC_6H_4Me\text{-}4)(CO)_2(\eta^5\text{-}C_2B_9H_9R_2)]^-$ (R = H, Me), whilst anionic, have frequencies not dissimilar to those of neutral **4** (Entry **1**) and **5** (Entry **2**), while the anionic docosohedral example $[W(\equiv CC_6H_4Me\text{-}4)(CO)_2(\eta^6\text{-}C_2B_{10}H_{10}Me_2)]^-$ has a considerably higher k_{CO} value 15.04 Ncm^{-1}. There is no correlation obvious to us between the net charge on the complex and derived WC bond orders or W≡C bond lengths for the carbyne ligand.

2.4. Sub-Series of Ligands

Tables 1 and 2 along with Figures 3 and 4 contain a number of as yet hypothetical derivatives that have yet to be prepared but which would appear to be entirely plausible based on the demonstrated viability of the ligands L in other systems. Some comments on sub-classes now follow.

2.4.1. Hydrotris(N-R^1-imidazolylidenyl)borates

Central to this communication are the tris(imidazolylidene)borates $HB(ImR^1)_3$. From Figure 3, it is clear that the ligand $HB(ImMe)_3$ occupies a position in a somewhat sparsely populated area of the electronic–steric map, being both strongly basic and also imparting considerable steric prophylaxis upon the carbonyl and carbyne co-ligands akin to that provided by the popular $HB(pzMe_2)_3$ ligand. The experimental and calculated values for k_{CO} are comparable to those for Stone's dicarbollide complexes (L = η^5-$C_2B_9H_9R_2$ R = H, Me) [79,88] which, however, carry a net negative charge, and so it must be assumed much of the negative charge resides within the carbaborane cage.

As expected, the $\%V_{bur}$ value for **4** is close to that of **5**. Smith has developed synthetic routes to the pro-ligand salts that carry *N*-substituents of varying bulk (^{t}Bu, Cy, $C_6H_2Me_3$-2,4,6) [4] and accordingly entries **1** (R^1 = Me, **4**), **35** (R^1 = Et), **36** (R^1 = ^{i}Pr), **37** (R^1 = ^{t}Bu) and **38** (R^1 = Ph) survey the sequential inclusion of increasing steric bulk at the position β to the metal. All attempts to geometrically minimize, or indeed even reasonably construct, the derivative with R^1 = mesityl met with spectacular failure, perhaps indicating a step too far, though this ligand has been successfully installed on four-coordinate nickel [37]. The phenyl derivative **38**, however, is able to accommodate unsubstituted aryl groups by allowing them to interdigitate between the carbonyl and carbyne ligands such that the aryl planes are near colinear with the W···B vector. A very approximate value for the $\%V_{bur}$ of 56.6% is provided by the hypothetical and implausible (distorted) octahedral complex $[WMe_3\{HB(ImMes)_3]$ (PM3tm level of theory). While it is not dissimilar to the value (59.8%) estimated for L = neutral $MeC(CH_2PPh_2)_3$ (**16**) and anionic $MeB(CH_2PPh_2)_3$ (**31**), inclusion of this excessive steric bulk would seem problematic. It should, however, be noted that a rich organometallic chemistry has emerged for the dihydro*bis*(*N*-

mesitylimidazolylidenyl)borate ligand coordinated to tantalum [33,34], for which the bidentate variant presents a considerably reduced steric impact, e.g., V_{bur} = 39.8% in pseudo-octahedral [$TaMe_4${$H_2B(ImMes)_2$}]. The trifluoromethylimidazolylidenyl derivate (Entry **39**) was also considered and found to be a rather modest net donor (ν_{CO} = 15.2 Ncm^{-1}) while presenting a comparatively occlusive encapsulating pocket (V_{bur} = 57.1%). The only currently available synthesis of *N*-trifluoromethylimidazole [111] is, however, not particularly amenable to the scales needed for an exploration of the $HB(ImCF_3)_3$ ligand. Figure 5 depicts the steric maps that arise from $\%V_{bur}$ calculations and shows the progression in steric encumbrance as the *N*-substituents are replaced along the alkyl series R^1 = Me, Et, ^{i}Pr, ^{t}Bu alongside those for R = Ph and CF_3.

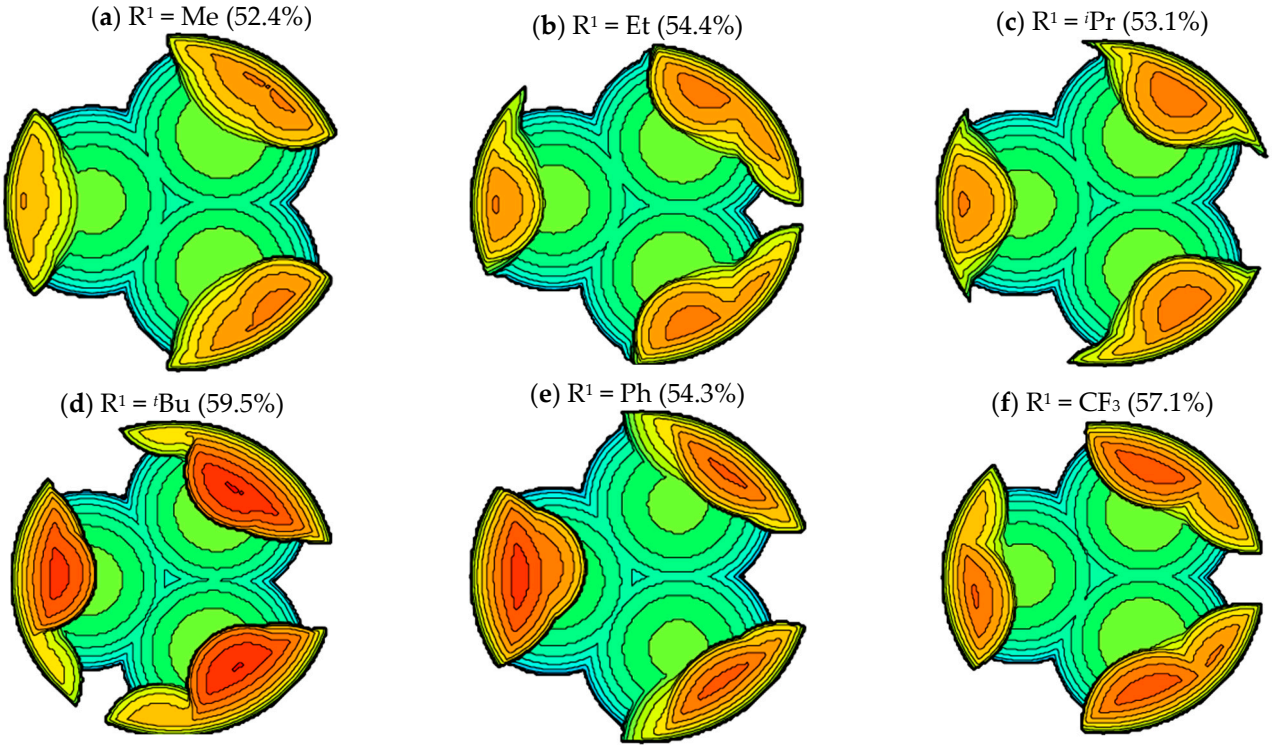

Figure 5. Steric maps [92,93] and $\%V_{bur}$ values in parentheses for a series of hydrotris(*N*-R^1-imidazolylidenyl)borates $HB(ImR^1)_3$ where (**a**) R^1 = Me; (**b**) R^1 = Et; (**c**) R^1 = ^{i}Pr; (**d**) R^1 = ^{t}Bu; (**e**) R^1 = Ph; (**f**) R^1 = CF_3.

What is immediately apparent from Figure 4 is that replacement of the 'parent' *N*-methylimidazole, which is both commercially available and cheap, with ethyl, iso-propyl or phenyl imidazoles actually results in very modest variation in the steric impact around the coordination sphere of the metal because the groups can direct their bulk away from the carbonyl and carbyne ligands. It is only with the ^{t}Bu (and to a lesser extent the CF_3) derivative that this bulk is unavoidably directed towards the metals centre. This is clear when the 3.5 Å value typically and arbitrarily employed in $\%V_{bur}$ calculations is replaced by 4.0, 5.0 and 6.0 Å (Figure 6), respectively. Thus, inclusion of phenyl, primary or secondary alkyl groups appears to have rather a modest steric influence directly on the metal coordination sphere but may contribute in a secondary manner to compound longevity by reducing the collisional cross section (Arrhenius pre-exponential factor) for proceeding reactions. It seems that only with tertiary alkyl (e.g., ^{t}Bu) or *ortho*-substituted aryl substituents (e.g., mesityl) that a significant impact on the steric profile is likely to manifest in the reactivity.

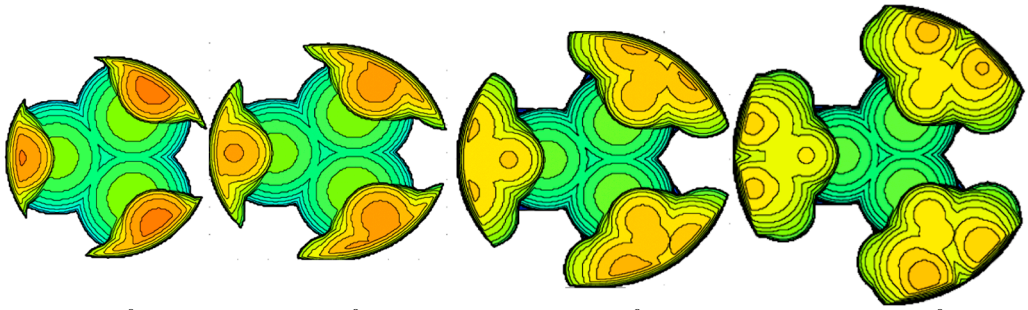

(**a**) 3.5 Å (**b**) 4.0 Å (**c**) 5.0 Å (**d**) 6.0 Å

Figure 6. Steric map dependence on radius of coordination sphere employed.

An intriguing question does, however, arise when the steric bulk is exaggerated, in that whilst this might be expected to increase the donor strength of the NHC:→W interaction, the inter-ligand repulsion is such that there is a notable increase in the W–C bond lengths of both the NHC donors cis (mean value) and trans to the carbyne (Table 3).

Table 3. Steric Impact of *N*-substituents in the Complexes [W(≡CC_6H_4Me)$(CO)_2${$HB(ImR)_3$}].

R	Mean W–C Å	Mean W–C_{cis} Å	W–C_{trans} Å	*TR* [a]
Me	2.262	2.226	2.335	1.049
CF_3	2.276	2.232	2.365	1.060
Et	2.268	2.233	2.339	1.047
^{i}Pr	2.268	2.232	2.341	1.049
Ph	2.277	2.237	2.357	1.054
^{t}Bu	2.349	2.312	2.424	1.048

[a] (W–C_{trans})/(Mean W–C_{cis}).

Thus, the simple σ-basicity vs. π-acidity of the free NHC is only part of the story if the metal–donor bond length increases (weakens?) significantly. This does not appear to be the case in the present system, in that while the ^{t}Bu derivative has especially long NHC–W bond lengths, it is nevertheless the most potent net donor (k_{CO} = 14.41 Ncm^{-1}) of all the ligands considered. In the case of the complexes [Ni(NO)(L)] where L represents a sub-set of ligands considered in Tables 1 and 2 (η^5-C_5Me_5, Tp*, $Hb(mt^{tBu})_3$ and $PhB(CH_2PPh_2)_3$ [112–116]) alongside those for selected tris(imidazolylidenyl)borates $RB(ImR^1)_3$ (R = H, Ph; R^1 = Me, ^{t}Bu, Mesityl, CH_2Cy [37]), Smith employed nitrosyl stretching frequency as a measure of the relative donor ability of 'L'. Similar σ-donor/π-acceptor arguments apply as they do to CO with the caveat that depending on the electronic nature of the metal centre, the nitrosyl may bend; i.e., lower values for ν_{NO} may indicate an electron rich metal centre *or* bending, which becomes more prevalent for late-transition metal centres with high *d*-occupancies [117]. In the case of four-coordinate nitrosyls of nickel, the situation is complicated by subtleties in the electronic nature of the nickel that remain moot [47,49]. While Smith was consistent in reporting data from the same essentially non-coordinating solvent toluene (or sometimes THF), data from other sources were acquired from a variety of media (not always stated) including the solid state (KBr, Nujol, $Ar_{(s)}$, etc.). The selenoimidazolylborate is a case in point for which the reported solid-state IR spectrum comprised two ν_{NO} bands [114]. Since the crystal structure revealed a single crystallographically independent molecule, one might assume the second vibrational mode was due to an alternative crystal modification in the bulk sample. Given the two bands differ by 11 cm^{-1} and the entire Tolman ν^T scale only spans 45 cm^{-1}, the importance of using solution derived data, preferably from a common solvent, is demonstrated.

2.4.2. Cyclopentadienyl Derivatives

In terms of percentage buried volume, the cyclopentadienyl ligand is somewhat unassuming (V_{bur} = 35.2%), and this is most commonly 'bulked out' via permethylation (**12**: L = C_5Me_5 V_{bur} = 42.4%), inclusion of trimethylsilyl substituents (**26**: L = $C_5H_3(SiMe_3)_2$ V_{bur} = 54.5%) or benzannulation with either one (**22**: L = indenyl V_{bur} = 37.3%) or two (**23**: L = fluorenyl V_{bur} = 40.4%) benzo rings. This imbues variable electron-releasing nature in the series $C_5H_3(SiMe_3)_2$ > C_5Me_5 > C_5H_5 ≈ fluorenyl > indenyl. A subtlety emerges from the geometry minimization of the indenyl derivative, which reveals a structural basis for Basolo's 'indenyl effect' [61,118,119]. Incipient ring slippage ($\eta^5 \rightarrow \eta^3$) might be inferred, given that the angle between the tungsten, the cyclopentadienyl ring centroid and the unique carbon atom is slightly acute (84.8°), such that the unique carbon (2.319 Å) and adjacent *pseudo* η^3-carbons (2.355, 2.352 Å) are noticeably closer to tungsten than are the benzo-fused carbons (mean: 2.534 Å). The C_6H_4 unit makes an angle of *ca* 5.9° with the three non-ring-fused carbons of the cyclopentadienyl ring. This slippage places the benzenoid ring trans to the carbyne ligand, as might be expected based on the characteristic trans influence of carbyne ligands. Experimentally acquired structural data are not currently available for indenyl, fluorenyl or bis(trimethylsilyl)cyclopentadienyl ligated carbynes through which to further explore this question, though enhanced reactivity in associative ligand addition reactions has been noted for the indenyl carbyne [Mo(≡$CC_6H_3Me_2$-2,6)$(CO)_2(\eta^5$-$C_9H_7)$] [61].

Although no examples exist of carbyne complexes bearing by the perchlorocyclopentadienyl ligand (**25**: L = η^5-C_5Cl_5), the tricarbido bimetallic complex [ReMn(μ_2-C_3)$(CO)_2$(NO)$(PPh_3)(\eta^5$-$C_5H_5)(\eta^5$-$C_5Cl_5)]^+$ described by Gladysz [120,121] might be viewed as possessing a degree of manganese carbyne character. Perchlorination results in a modest increase in the steric bulk of the ligand (40.8 cf. 42.4% for η-C_5Me_5) but a quite substantial decrease in donor ability (k_{CO} = 15.51 Ncm^{-1}). Perphenylation, in contrast, has only a modest effect on the net basicity of the ligand (k_{CO} = 15.34 Ncm^{-1}), while the buried volume increases significantly (V_{bur} = 48.3%) due to the requisite orientation of the aryl groups to near orthogonal to the cyclopentadienyl plane. The tetraphenylcyclopentadienyl carbyne complex [W(≡CPh)$(PPh_2C_6H_4CH$=CHPh)$(\eta^5$-$C_5HPh_4)$] [122] and a single rather exotic pentaphenylcyclopentadienyl complex [W(≡CPh)(NCMe)$(\eta^2$-$C_{60})(\eta^5$-$C_5Ph_5)$] [123] have been described.

2.4.3. Arene Derivatives

While hexahapto arene co-ligated carbyne complexes such as **18**, **20** and **21** appear unknown, a manifold of intriguing molybdenum carbyne complexes bearing the $C_6H_4(C_6H_4P^iPr_2$-2)$_2$-1,4 trans-coordinating diphosphine have been shown by Agapie to enter into variable degrees of arene-molybdenum interaction during transformations that demonstrate the interplay of carbyne and carbido ligands [124–127]. It therefore seems reasonable to anticipate that compounds akin to Entries **18**, **20** and **21** will emerge. It is apparent that conclusions similar to those for cyclopentadienyl substituents will result, except that the overall complex bears a positive charge, providing a point of connection with group 7 carbynes [M(≡CR)$(CO)_2(\eta^5$-$C_5H_5)]^+$ (M = Mn, Re) [128–132]. The hexaethylbenzene derivative **21** would appear to present a sterically quite encapsulating environment (V_{bur} = 53.3%) cf. the hexamethyl analogue (V_{bur} = 45.9%) due to the 3-up/3-down mutual disposition of the ethyl substituents. This feature has been employed to favour unusual regiochemistry in selective alkane binding by the 'W$(CO)_2(\eta^6$-$C_6Et_6)$' fragment [133]. Finally, we note that the inorganic benzene $B_3N_3Me_3$ has, as expected, a steric profile similar (V_{bur} = 46.2%) to that of C_6Me_6 (V_{bur} = 45.9%), and the non-planar ring is a comparable net donor to the tungsten centre (k_{CO} = 15.84 Ncm^{-1} vs. 15.85 Ncm^{-1} for **20**). This is also implicit from infrared data for [Cr$(CO)_3(\eta^6$-$B_3N_3Me_6)$] (Cyclohexane: ν_{CO} = 1963, 1867 cm^{-1}) vs. [Cr$(CO)_3(\eta^6$-$C_6Me_6)$] (ν_{CO} = 1962, 1888 cm^{-1}) provided in a publication in which Werner indicated that [W$(CO)_3(\eta^6$-$B_3N_3Me_6)$] also appeared viable [134,135].

2.4.4. Pnictolyl Ligands

Schrock has explored the utility of high oxidation state carbene and carbyne complexes ligated by σ- and η^5-pyrollyl ligands [136], though low oxidation variants have yet to emerge. Carbynes ligated by the heavier pnictolyl ligands η^5-AC_4R_4 (A = P, As), however, remain unknown, though both ligands have been shown to serve as ersatz cyclopentadienyls [137–140]. With the ready availability of synthetic routes to anionic pnictolyl reagents, it may be presumed that complexes of the form $[M(\equiv CR)(CO)_2(\eta^5\text{-}AC_4R'_4)]$ (A = P, As, Sb) will emerge in the future, given that, like carbynes, arsolyl ligands have been shown to support intermetallic bonding [141–143].

2.4.5. Toluidyne Orientation

Perusal of the structures, experimentally or computationally derived, reveals a broad range of orientations of the toluidine ring with respect to the nominal coordination axes. This is of secondary importance in that for all examples, the ^{1}H NMR spectra involve a simple AA'BB' pattern indicating free rotation on the ^{1}H NMR (and ^{13}C) NMR timescale(s). Arbitrarily adopting the cationic carbyne formalism ($[CF]^+$, $[NO]^+$ and CO being isoelectronic molecules), coordinated to a d^6-ML_5 fragment, the two carbyne acceptor orbitals vary in energy by only 0.2 eV, as do the two metal retrodative orbitals (HOMO-1, HOMO-2) of, e.g., the 'W(CO)$_2$(Tp)' fragment (Figure 7). The HOMO itself is invariably associated with metal–carbonyl π-bonding and is orthogonal (δ-symmetry) to the W–Carbyne vector. Accordingly, any conformational preference should be presumed to reflect interligand steric factors and/or intermolecular packing effects. For the majority of structurally characterized carbyne complexes of the M(CO)$_2$(Tp*) fragment; for example, the carbyne substituent typically nestles between two dimethylpyrazolyl groups. NB: The molecular orbitals of the actual carbyne complex are, as they must be, independent of the arbitrary electron allocation to hypothetical constituent fragments; i.e., similar interpretation based on $[CC_6H_4Me]^{3-}$ and d^2-ML_5^{3+} or neutral CC_6H_4Me-4 and d^5-ML_5 deconstructions lead to the same conclusion.

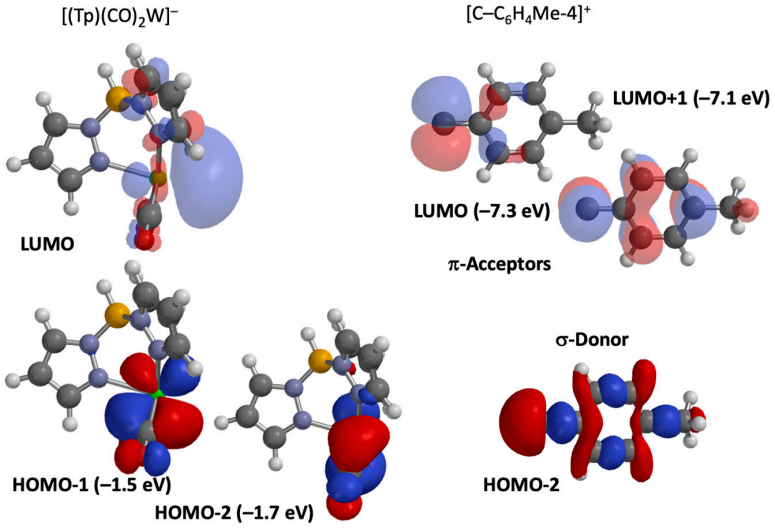

Figure 7. Valence orbitals of the hypothetical $[CC_6H_4Me\text{-}4]^+$ and d^6-$[W(CO)_2(Tp)]$ fragments.

2.5. A Heterobimetallic Hydrotris(imidazolylidenyl)borate Complex

To date, the tris(imidazolylidenyl)borate class of ligands has only been employed in monometallic systems; however, terminal carbyne ligands have an extensively documented propensity to support metal–metal bond formation, as championed by Stone [144]. In particular, the addition of gold(I) reagents to monometallic carbyne complexes [145–155] is of interest due to the tendency of the carbyne to adopt a semi-bridging rather than the more common symmetrical bridging geometry. This is considered to arise when the carbyne bridges electronically disparate metals, and therefore, the late high *d*-occupancy

metal (d^{10} gold(I) or platinum(0)) is considered to act as a σ-donor (*Z*-type metal–ligand bonding [156]) to the carbyne carbon. Accordingly, the reaction of **4** with [AuCl(SMe$_2$)] was investigated and found to readily provide the bimetallic complex [WAu(μ-CC$_6$H$_4$Me-4)Cl(CO)$_2${HB(ImMe)$_3$}] (**6**, Scheme 4). The complex is somewhat unstable in solution, slowly depositing elemental gold during unsuccessful attempts to slowly obtain crystallographically serviceable crystals. The formulation, however, rests reliably on spectroscopic data which may be compared with precedents for other carbyne and tungsten substituents. The reaction is accompanied by a shift in the ν_{CO} absorptions to a higher frequency (CH_2Cl_2: 1971, 1879 cm^{-1}) than those of the precursor in the same solvent (1958, 1873 cm^{-1}). The carbyne carbon resonance in the $^{13}C\{^1H\}$ NMR spectrum appears at δ_C = 277.7, and while this is only marginally shifted from that of the precursor (280.7 ppm), there is a dramatic decrease in the value of $^1J_{WC}$ (85 Hz cf. 171.3 Hz for **4**), which is consistent with the increase coordination number (reduced *s*-character) of both tungsten and carbon. The resonances due to the imidazolylidene donors appear at 187.7 [$^1J_{CW}$ = 90 Hz], 173.7 [$^1J_{CW}$ = 71 Hz] in a similar region to the precursor but with more similar values for $^1J_{WC}$ (90, 71 Hz) once the trans influence of the carbyne is alleviated upon gold adduct formation.

While the ^1H and $^{13}C\{^1H\}$ NMR spectra each confirm a locally C_s symmetric environment around the tungsten, at least on these timescales, they do not distinguish between the AuCl unit lying syn or anti to the imidazolylidene units; however, based on precedent from the sterically similar HB(pzMe$_2$)$_3$ ligand, it seems likely that the AuCl unit nestles between two imidazolylidene rings. This geometry was adequately modelled (Figure 8) at the ωB97X-D/6-31G/LANL2Dζ/gas-phase level of DFT, from which it would appear that the W–C bond clearly retains its considerable multiple-bond character (W–C = 1.913 Å). The W–C–C (148.9°) and Au–C–C (121.5°) angles indicate semi rather than symmetrical bridging such that the C–C and W–Au vectors form an obtuse angle of 101.4°. Despite numerous (>80) examples of structurally authenticated W–Au bonds, only two have bonds that are not supported by bridging ligands, viz. the compounds [WAu(CO)$_3$(PPh$_3$)(η^5-C$_5$H$_4$R)] (R = H 2.698 Å [157] and $CH_2CH_2NHMe_2^+Cl^-$ 2.712 Å [158]). The optimized Au–W bond length for **6** (2.812 Å) is therefore comparable to these, though towards the longer end of the range. The infrared ν_{CO} absorptions are noted at 1955 and 1899 cm^{-1} (λ_2), while TD-DFT analysis suggests that the colour of the complex may be attributed to absorptions calculated at 420 nm (W–C ≈ *z*-axis: HOMO-LUMO; d_{xy}-W=Cπ*), 357 (HOMO-LUMO+1; d_{xy}-WAuσ*) and 344 nm (HOMO-1-LUMO; W=Cπ-W=Cπ*), the first two of which involve considerable charge transfer.

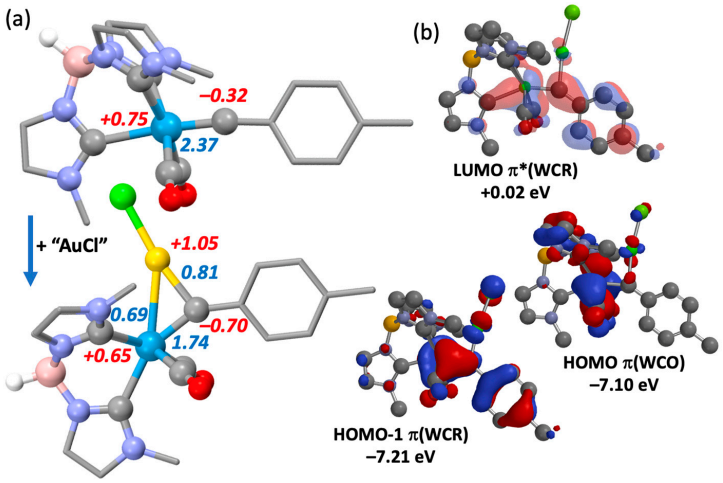

Figure 8. (**a**) Optimized geometries of [W(≡CC$_6$H$_4$Me-4)(CO)$_2${HB(ImMe)$_3$}] (**4**) and the heterobimetallic complex [WAu(μ-CC$_6$H$_4$Me-4)Cl(CO)$_2${HB(ImMe)$_3$}] (**6**) indicating changes in Löwdin bond order (blue) and natural atomic charge (red) upon 'AuCl' adduct formation (ωB97X-D/6-31G*/LANL2Dζ, hydrogen atoms omitted, tolyl and imidazolyl groups simplified). (**b**) Frontier molecular orbitals of interest for **6** at Isovalue = 0.032 $\sqrt{(e/au^2)}$.

3. Experimental

3.1. General Considerations

Experimental work was performed using standard Schlenk techniques with pure dry nitrogen or argon, or in an argon atmosphere glovebox, unless otherwise specified. All solvents used in the syntheses were dried and degassed. Unless otherwise indicated, reagents were used as received from commercial suppliers.

Infrared data were obtained using a Shimadzu FTIR-8400 for solutions and a Perkin Elmer FTIR Spectrum 2 for solid-state ATR measurements. NMR spectra were measured using Bruker Avance 400, Bruker Avance 600 or Bruker Avance 800 spectrometers at the temperatures indicated. Chemical shifts (δ) are reported in ppm with coupling constants in Hz, all referenced to the appropriate solvent resonance. Multiplicities indicated do not include the satellites for the ^{183}W isotopomers, the couplings for which are listed separately. Positive ion high-resolution electrospray ionisation mass spectroscopy (ESI) data were provided by the ANU Research School of Chemistry Joint Mass Spectrometry team; an acetonitrile matrix was used for all samples. Single-crystal X-ray diffraction (XRD) crystallographic data were acquired with a SuperNova CCD diffractometer using Mo-Kα radiation (λ = 0.71073 Å), employing CrysAlis PRO software [159] (https://www.agilent.com/ accessed on 20 November 2023), refined with Olex2 [160], and structural models were depicted using Mercury [161]. Elemental microanalytical data were not acquired [162].

Computational studies were performed using the *SPARTAN20* suite of programs [40]. Cyclic voltammetry (CV) was performed using a PalmSens 4 Potentiostat/Galvanostat/Impedance Analyser and carried out in a single-compartment 3-electrode glass cell, with a 3 mm glassy carbon working electrode, platinum wire counter electrode and silver wire pseudo-reference electrode. Analyte solutions were prepared at 1 mM in dichloromethane with 0.1 M [NBu_4][PF_6] supporting electrolyte. Solutions were sparged with N_2 bubbled through dichloromethane prior to measurements, then maintained under an atmosphere of N_2 during voltammetry. All measurements were referenced to ferrocene, which was added to the solution following each measurement.

Infrared and NMR spectra for all new compounds are provided in the accompanying Supplementary Materials.

*3.2. Synthesis of [W(≡CC$_6$H$_4$Me-4)(CO)$_2$(pic)$_2$(Br)] (**2a**)*

Note: the following synthesis is a modified version of the synthesis of cis,cis,trans-[W(≡CC$_6$H$_3$Me$_2$-2,6)(CO)$_2$(pic)$_2$Br] [15]. A solution of 4-bromotoluene (6.568 g, 38.40 mmol) in diethyl ether (60 mL) was cooled to 0 °C before lithium (0.618 g, 89.0 mmol, hammered and cut wire) was added. This was stirred vigorously at 0 °C for 30 min before being allowed to slowly warm to room temperature and being stirred for a further 3 h. The lithium reagent was added dropwise to a suspension of [W(CO)$_6$] (8.445 g, 24.00 mmol) in diethyl ether (60 mL) until IR spectroscopy indicated no [W(CO)$_6$] remained. The red solution was cooled to –78 °C before trifluoroacetic anhydride (3.40 mL, 24.3 mmol) was added dropwise over a period of 10 min, resulting in a yellow precipitate. After stirring for 30 min at –78 °C, 4-picoline (6.0 mL, 62 mmol) was added. The suspension was allowed to slowly warm to room temperature and stirred overnight. The yellow precipitate was isolated via cannula filtration and extracted with dichloromethane (60 mL) and the combined extracts were filtered through diatomaceous earth, followed by washing with further dichloromethane until the extracts were colourless (total volume 200 mL). The solvent volume was reduced to *ca* 40 mL under reduced pressure before slow dilution with hexane (300 mL) to precipitate a yellow-orange solid that was freed of supernatant via cannula filtration. Hexane (80 mL) was added, and the suspension was ultrasonically triturated for 10 min to remove residual [W(CO)$_6$]. The yellow-orange solid was collected on a sinter, washed with further hexane (20 mL) and dried under high vacuum (13.094 g, 21.446 mmol, 89% isolated yield).

IR (CH_2Cl_2, cm^{-1}): 1986 vs. ν_{CO}, 1897 vs. ν_{CO}. **IR** (ATR, cm^{-1}): 1970 vs. ν_{CO}, 1881 vs. ν_{CO}.**^{1}H NMR** (600 MHz, CD_2Cl_2, 298 K) δ_H = 8.91 [d, 4 H, $^3J_{HH}$ = 7, H^{2,6}(pic)], 7.25 [d, 2 H, $^3J_{HH}$ = 8, H^{2,6}(C_6H_4)], 7.13 [d, 4 H, $^3J_{HH}$ = 7, H^{3,5}(pic)], 7.09 [d, 2 H, $^3J_{HH}$ = 9, H^{3,5}(C_6H_4)], 2.38 [s, 6 H, pic-CH_3], 2.29 [s, 3 H, tolyl-CH_3]. **^{13}C{^{1}H} NMR** (151 MHz, CD_2Cl_2, 298 K)

δ_C = 263.9 [$^1J_{WC}$ = 203 Hz, W≡C], 221.4 [$^1J_{WC}$ = 169 Hz, CO], 153.3 [$C^{2,6}$(pic)], 151.0 [C^4(pic)], 146.9 [$C^1(C_6H_4)$], 138.5 [$C^4(C_6H_4)$], 129.4 [$C^{2,6}(C_6H_4)$], 129.1 [$C^{3,5}(C_6H_4)$], 126.3 [$C^{3,5}$(pic)], 21.8 [tolyl-CH_3], 21.3 [pic-CH_3]. **MS** (ESI, +ve ion, *m*/*z*): Found: 609.0375. Calcd for $C_{22}H_{22}N_2O_2{}^{79}Br^{184}W$ [M + H]$^+$: 609.0374. Crystals suitable for structural determination were grown from liquid diffusion of diethyl ether into a saturated dichloromethane solution of the sample at -20 °C. **Crystal Data** for $C_{22}H_{21}BrN_2O_2W.(OEt_2)_{0.5}$ (M_w= 646.23 gmol^{-1}): monoclinic, space group *C*2/c (no. 15), *a* = 23.3477(7) Å, *b* = 12.5106(2) Å, *c* = 17.9409(5) Å, *β* = 110.628(3) °, *V* = 4904.4(2) Å^3, *Z* = 8, *T* = 150.0(1) K, μ(Mo *K*α) = 6.364 mm^{-1}, D_{calc} = 1.750 Mgm^{-3}, 37431 reflections measured (7.422° ≤ 2Θ ≤ 64.280°), 8075 unique which were used in all calculations. The final R_1 was 0.0311 ($I > 2\sigma(I)$) and wR_2 was 0.0671 (all data) with 291 refined parameters with one restraint, CCDC 2305468. The molecular geometry in the solid state is depicted in Figure 9.

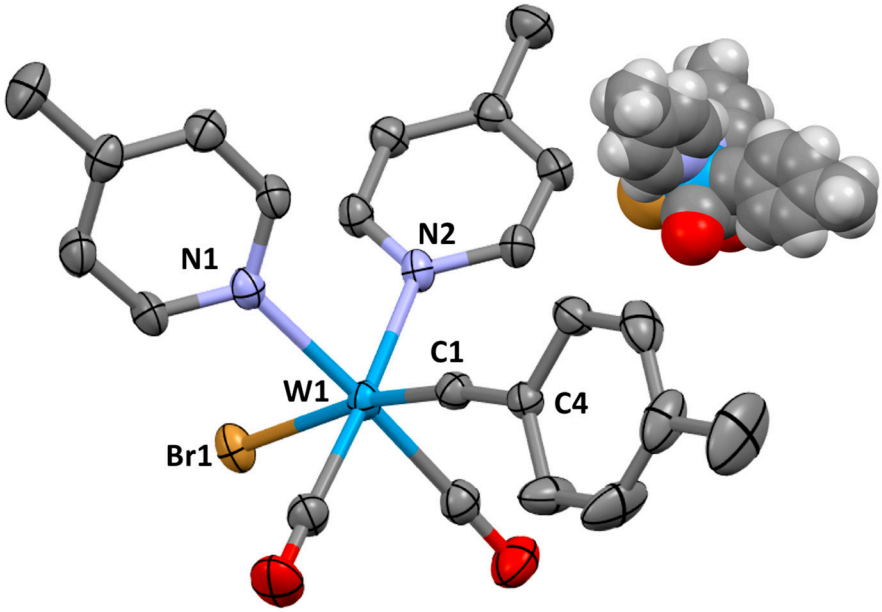

Figure 9. Molecular structure of cis,cis,trans-[W(≡CC_6H_4Me-4)$(CO)_2$(pic)$_2$(Br)] in a crystal (50% displacement ellipsoids, hydrogen atoms omitted for clarity).

*3.3. Synthesis of [Mo(≡CC_6H_4Me-4)$(CO)_2$(pic)$_2$(Br)] (**2b**)*

A solution of 4-bromotoluene (6.842 g, 40.00 mmol) in diethylether (50 mL) was cooled to 0 °C before lithium (1.3 g, 190 mmol, hammered and cut wire) was added. This was stirred vigorously at 0 °C for 30 min before being allowed to slowly warm to room temperature and being stirred for a further 3.5 h. The lithium reagent was added dropwise to a suspension of [$Mo(CO)_6$] (6.338 g, 24.01 mmol) in diethyl ether (60 mL) until negligible [$Mo(CO)_6$] remained, as indicated by in situ IR spectroscopy. The red solution was cooled to –78 °C before trifluoroacetic anhydride (3.40 mL, 24.3 mmol) was added dropwise over a period of 10 min. After being stirred for 45 min at –78 °C, 4-picoline (6.0 mL, 62 mmol) was added. The suspension was allowed to slowly warm to room temperature and stirred overnight. The yellow precipitate was isolated via cannula filtration and extracted with dichloromethane (50 mL) and the extracts filtered through diatomaceous earth, followed by washing with further dichloromethane (6 × 5 mL). The volume was reduced to 50 mL under reduced pressure before slow dilution with hexane (120 mL) to precipitate a yellow solid that was freed of supernatant via cannula filtration and dried under high vacuum (8.473 g, 16.25 mmol, 68% isolated yield).

IR (CH_2Cl_2, cm^{-1}): 2000 vs. ν_{CO}, 1918 vs. ν_{CO}. **IR** (ATR, cm^{-1}): 1986 vs. ν_{CO}, 1913 vs. ν_{CO}. **^{1}H NMR** (600 MHz, CD_2Cl_2, 298 K) δ_H = 8.87 [d, 4 H, $^3J_{HH}$ = 6, $H^{2,6}$(pic)], 7.36 [d, 2 H, $^3J_{HH}$ = 8, $H^{2,6}(C_6H_4)$], 7.08-7.14 [m, 6 H, $H^{3,5}$(pic) and $H^{3,5}(C_6H_4)$ over-lapped], 2.37 [s, 6 H, pic-CH_3], 2.32 [s, 3 H, tolyl-CH_3]. **^{13}C{^{1}H} NMR** (151 MHz, CH_2Cl_2, 298 K)

δ_C = 276.8 [Mo≡C], 224.4 [CO], 152.9 [$C^{2,6}$(pic)], 150.6 [C^4(pic)], 143.5 [$C^1(C_6H_4)$], 139.5 [$C^4(C_6H_4)$], 129.3 [$C^{3,5}(C_6H_4)$], 129.2 [$C^{2,6}(C_6H_4)$], 125.9 [$C^{3,5}$(pic)], 21.8 [tolyl-CH_3], 21.26 [pic-CH_3)]. **MS** (ESI, +ve ion, *m/z*): Found: 443.0659. Calcd for $C_{22}H_{22}N_2O_2{}^{98}Mo$ $[M - Br]^+$: 443.0662.

3.4. Synthesis of [Tris(1-methylimidazolium)borate] Bis(hexafluorophosphate) ([1](PF$_6$)$_2$)

A 1 L three-necked flask was fitted with a stirrer bar, water-cooled reflux condenser, pressure-equalizing dropping funnel and a gas outlet leading to a NaOH scrubber. The entire apparatus was flushed with nitrogen for 30 min before trimethylamine-borane complex (7.32 g, 100 mmol) was added, followed by 150 mL degassed chlorobenzene. To the dropping was added 50 mL chlorobenzene and bromine (7.8 mL, 85 mmol Br_2). The bromine solution was added to the flask at a rate of about one drop/second whilst the reaction was flushed with a gentle stream of nitrogen. This reaction is initially very exothermic and the rate of bromine addition should be adjusted accordingly; caution should also be exercised, since hydrogen gas is also liberated at this stage. After approximately half of the bromine had been added, the exothermicity was less pronounced and rate of addition of the remainder could be increased safely. The mixture was then stirred for 3 h at ambient temperature, during which time the orange colour of bromine slowly faded to a pale yellow. Hydrogen bromide was liberated during this time as nitrogen was continuously swept over the reaction. *N*-methylimidazole (28 mL, 330 mmol) was added to the mixture, and the apparatus was carefully transferred to a heating mantle, where it was brought to reflux for 4-6 h. Upon heating, a white crystalline solid precipitated from the reaction mixture; extended heating is to be discouraged, as this leads to the formation of tarry yellow materials and poor yields of product. The chlorobenzene layer was decanted from the solids while warm, and the flask was then rinsed with 3 × 100 mL portions of toluene; the washings were subsequently discarded. The white solid was dissolved into 100 mL methanol and added slowly to a vigorously stirred solution of $NaPF_6$ (35 g, 210 mmol; $NaBF_4$ may also be used) in 100 mL methanol, from which the product precipitated as a fluffy white solid. The white solids were collected via filtration, washed with 3 × 50 mL portions each of methanol and Et_2O and dried under suction. Purity was sufficient for synthetic purposes, though an analytically pure sample was obtained via re-crystallisation from acetone/Et_2O (vapour diffusion). Isolated yield 11.50 g (21 mmol, 21%) as the PF_6 salt or 12.90 g (30 mmol, 30%) as the BF_4 salt.

IR (THF, cm^{-1}): 2454 w ν_{BH}. **IR** (ATR, cm^{-1}): 2455 vs. ν_{BH}, 827 vs. ν_{PF}. ^{1}H NMR (400 MHz, CD_3CN, 25 °C): δ_H = 8.17 (s, 3 H, N_2CH), 7.38 (t, $^3J_{HH}$ = 1.7 Hz, 3 H, NCHCH), 7.17 (t, $^3J_{HH}$ = 1.7 Hz, 3 H, NCHCH), 3.87, (s.br, 1 H, BH), 2.18 (s, 9 H, NCH_3). **^{13}C{^{1}H} NMR** (101 MHz, CD_3CN, 25 °C): δ_C= 139.9 (N_2C), 125.6 (NCC), 124.2 (NCC), 36.4 (NCH_3). ^{11}B{^{1}H} NMR (128 MHz, CD_3CN, 25 °C): δ_B = −3.50 (BH). **^{11}B NMR** (128 MHz, CD_3CN, 25 °C): δ_B = −3.42 (d, $^1J_{BH}$ = 121.7 Hz, BH). ^{19}F NMR (376 MHz, CD_3CN, 25 °C): δF = −72.9 (d, $^1J_{PF}$ = 708 Hz, PF_6). **^{31}P{^{1}H} NMR** (162 MHz, CD_3CN, 25 °C): δ_P = −144.6 (sept, $^1J_{PF}$ = 700 Hz, PF_6). **MS** (ESI, +ve ion, *m/z*): Found: 257.1685. Calcd for $C_{12}H_{18}N_6{}^{11}B$. $[M–H]^+$: 257.1686. **Crystal Data** for $C_{12}H_{19}BF_{12}N_6P_2$ (M_w = 548.08 $gmol^{-1}$): monoclinic, space group $P2_1/n$ (no. 14), a = 20.7403(2) Å, b = 10.10590(10) Å, c = 20.7879(2) Å, β = 97.4530(10)°, V = 4320.32(7) Å^3, Z = 8, T = 150.2(1) K, μ(CuKα) = 2.945 mm^{-1}, D_{calc} = 1.685 Mgm^{-3}, 54277 reflections measured (5.664° ≤ 2Θ ≤ 156.216°), 9112 unique (R_{int} = 0.0625, R_{sigma} = 0.0400), which were used in all calculations. The final R_1 was 0.0603 ($I > 2\sigma(I)$) and wR_2 was 0.1725 (all data) for 711 refined parameters with 296 restraints. CCDC 2305467.

*3.5. Synthesis of [W(≡CC$_6$H$_4$Me-4)(CO)$_2${HB(ImMe)$_3$}] (**4**)*

Tris(1-methylimidazolium)borate bis(hexafluorophosphate) ([1](PF$_6$)$_2$: 0.400 g, 0.730 mmol) was dissolved in tetrahydrofuran (30 mL) and cooled (dry ice/propanone). A solution of *n*-butyllithium (1.40 mL, 1.6 M, 2.20 mmol, hexanes) was added dropwise at –78 °C. While being stirred for 90 min at this temperature, the solution became pale yellow, at which point solid

[W(≡CC_6H_4Me-4)$(CO)_2$(γ-pic)$_2$(Br)] (**2a**: 0.45 g, 0.70 mmol) was added. After it was stirred at this temperature for 15 min, the mixture was allowed to warm to room temperature and stirred for a further 3 h and then freed of volatiles under reduced pressure. The residual black tar was dissolved in a minimum of dichloromethane (~5mL) and subjected to flash column chromatography (silica gel, N_2, CH_2Cl_2). The orange band that eluted first was collected, and the solvent was removed under reduced pressure to give (**4**) a bright orange powder. Yield: 0.11 g (0.18 mmol, 20%).

IR (CH_2Cl_2, cm^{-1}): 2453 w ν_{BH}, 1958 vs. ν_{CO}, 1873 vs. ν_{CO}. **IR** (ATR, cm^{-1}): 2442 w ν_{BH}, 1949 vs. ν_{CO}, 1867 vs. ν_{CO}. **^{1}H NMR** (800 MHz, CD_2Cl_2, 25 °C): δ_H = 7.36 [d, $^3J_{HH}$ = 7.4 Hz, 2 H, $H^{2,6}(C_6H_4)$], 7.11 [d, $^3J_{HH}$ = 1.4 Hz, 2 H, NCHCH], 7.08 (d, $^3J_{HH}$ = 1.5 Hz, 1 H, NCCH], 7.07 [d, $^3J_{HH}$ = 7.0 Hz, 2 H, $H^{3,5}(C_6H_4)$], 6.84 [d, $^3J_{HH}$ = 1.4 Hz, 2 H, NCCH], 6.76 [d, $^3J_{HH}$ = 1.3 Hz, 1 H, NCCH], 3.80 [s, 3 H, NCH_3), 3.79 [s, 6 H, NCH_3], 2.26 [s, 3 H, CCH_3]. **^{13}C{^{1}H} NMR** (201 MHz, CD_2Cl_2, 25 °C): δ_C = 280.7 [$^1J_{CW}$ = 171.3 Hz, W≡C], 223.3 [$^1J_{CW}$ = 132.1 Hz, CO], 192.5 [$^1J_{CW}$ = 95.0 Hz, NCN)], 181.7 [$^1J_{CW}$ = 44.7 Hz, NCN], 151.5 [$^2J_{CW}$ = 39.1 Hz, $C^4(C_6H_4)$], 136.9 [$C^{2,6}(C_6H_4)$], 129.0 [$C^{3,5}(C_6H_4)$], 128.8 [$C^4(C_6H_4)$], 124.3 [$C^5(C_3N_2H_2)$], 123.7 [$C^5(C_3N_2H_2)$), 120.7 [$C^4(C_3N_2H_2)$], 120.3 [$C^4(C_3N_2H_2)$], 38.8 [NCH_3], 38.1 [NCH_3], 21.8 [CCH_3]. **^{11}B{^{1}H} NMR** (128 MHz, $CDCl_3$, 25 °C): δ_B = −1.41 (BH). **^{11}B NMR** (128 MHz, $CDCl_3$, 25 °C): δ_B = −1.35 (d, $^1J_{BH}$ = 97.9 Hz, BH). **MS** (ESI, +ve ion, *m*/*z*): Found: 599.1572. Calcd for $C_{22}H_{24}{}^{11}BN_6O_2{}^{184}W$. $[M + H]^+$: 599.1563. **CV** (CH_2Cl_2): $E_{\frac{1}{2}}$ = 0.00 V vs. $[Fe(C_5H_5)_2]/[Fe(C_5H_5)_2]^+$. See Figure 8 for computationally optimized molecular structure.

3.6. Synthesis of [W(≡CC_6H_4Me-4)$(CO)_2$(Tp)] (**5**)*

The complex has been previously described via the reaction of the thermolabile intermediate [W(≡CC_6H_4Me-4)Br$(CO)_4$] (from [W{=C(OMe)C_6H_4Me-4}$(CO)_5$] and BBr_3) and K[Tp*] (80%) [17]. The present synthesis follows a similar approach to the synthesis of [W(≡$CC_6H_3Me_2$-2,6)$(CO)_2$(Tp)] [17]. Sodium hydrotris(3,5-dimethyl-1-pyrazolyl) borate (0.183 g, 0.544 mmol) was dissolved in dichloromethane (15 mL) and added to a solution of [W(≡CC_6H_4Me-4)$(CO)_2$(γ-pic)$_2$(Br)] (**2a**: 0.307 g, 0.506 mmol) in dichloromethane (20 mL) with stirring overnight. The solution slowly darkened from pale orange to dark red, and this transition was visible after 3 h. Solvent and picoline were removed under reduced pressure, and the residue was redissolved in a minimum of dichloromethane (~2mL) and purified via flash column chromatography using a 1:2 DCM to petroleum spirits 60–80 eluent (silica gel, N_2). The orange fraction which eluted first was collected, and solvent was removed under reduced pressure to give (**5**) a bright orange powder. Yield: 217 mg (0.339 mmol, 67%). **IR** (CH_2Cl_2, cm^{-1}): 2554w ν_{BH}, 1971 vs. ν_{CO}, 1879 vs. ν_{CO}. **IR** (ATR, cm^{-1}): 2550 w ν_{BH}, 1954 vs. ν_{CO}, 1861 vs. ν_{CO}. **^{1}H NMR** (800 MHz, $CDCl_3$, 25 °C): δ_H = 7.36 [d, $^3J_{HH}$ = 7.4 Hz, 2 H, $H^{2,6}(C_6H_4)$], 7.10 [d, $^3J_{HH}$ = 7.9 Hz, 2 H, $H^{3,5}(C_6H_4)$], 5.89 [s, 2 H, H^4(pz)], 5.79 [s, 1 H, H^4(pz)], 2.52 [s, 6 H, pzCH_3], 2.47 [s, 3 H, pzCH_3], 2.38 [s, 6 H, pzCH_3], 2.35 [s, 3 H, pzCH_3], 2.31 [s, 3 H, $C_6H_4CH_3$). **^{13}C{^{1}H} NMR** (201 MHz, $CDCl_3$, 25 °C): δ_C = 279.2 [$^1J_{CW}$ = 186.3 Hz, W≡C], 224.0 [$^1J_{CW}$ = 166.5 Hz, CO], 152.4 [C^5(pz)], 152.1 [C^5(pz)], 148.0 [$^2J_{CW}$ = 42.5 Hz, $C^1(C_6H_4)$], 145.7 [C^3(pz)], 144.5 [C^3(pz)], 137.8 [$C^{2,6}(C_6H_4)$], 129.3 [$C^{3,5}(C_6H_4)$], 128.8 [$C^4(C_6H_4)$], 106.7 [C^4(pz)], 106.5 [C^4(pz)], 21.8 [$C_6H_4CH_3$], 16.7 [pzCH_3], 15.4 [pzCH_3], 12.8 [pzCH_3], 12.8 [pzCH_3)]. **^{11}B{^{1}H} NMR** (128 MHz, $CDCl_3$, 25 °C): δ_B = −9.17 (BH). **^{11}B NMR** (128 MHz, $CDCl_3$, 25 °C): δ_B = −9.15 (br, BH). **MS** (ESI, +ve ion, *m*/*z*): Found: 641.2039. Calcd for $C_{25}H_{30}{}^{11}BN_6O_2{}^{184}W$ 641.2033. $[M + H]^+$. **CV** (CH_2Cl_2): $E_{\frac{1}{2}}$ = 0.18 V vs. $[Fe(C_5H_5)_2]/[Fe(C_5H_5)_2]^+$.

*3.7. Synthesis of [WAu(μ$_2$-CC_6H_4Me-4)Cl$(CO)_2${HB(ImMe)$_3$}] (**6**)*

To a solution of [W(≡CC_6H_4Me-4)$(CO)_2${HB(ImMe)$_3$}] (**4**: 20 mg, 0.033 mmol) in dichloromethane (5 mL) was added [AuCl(SMe_2)] (10 mg, 0.034 mmol) with stirring, whereupon the solution turned from bright orange to dark red. After 30 min, a further equivalent of [AuCl(SMe_2)] (10 mg, 0.034 mmol) was added to the reaction, which was stirred for a further 15 min (longer reaction times resulted in gold mirror formation). After this

time, the resulting solution was subjected to flash column chromatography (diatomaceous earth, CH_2Cl_2, N_2) to collect the bright orange fraction, from which solvent was removed under reduced pressure. The resulting dark orange powder was suspended in n-hexane (10 mL) and then collected via vacuum filtration, washed with n-hexane (3 × 5 mL) and dried in vacuo for 45 min, to give a brown-gold powder of (**6**). Yield: 14 mg (8.7 μmol, 54%). **IR** (CH_2Cl_2, cm^{-1}): 2455 w ν_{BH}, 1986 vs. ν_{CO}, 1911 vs. ν_{CO}. **IR** (ATR, cm^{-1}): 2454 w ν_{BH}, 1983 vs. ν_{CO}, 1879 vs. ν_{CO}.**^{1}H NMR** (600 MHz, CD_2Cl_2, 25 °C): δ_H = 7.87 [d, $^3J_{HH}$ = 8.1 Hz, 2 H, $H^{2,6}(C_6H_4)$]), 7.24 [d, $^3J_{HH}$ = 7.8 Hz, 2 H, $H^{3,5}(C_6H_4)$], 7.20 [d, $^3J_{HH}$ = 1.6 Hz, 2 H, NCCH], 7.14 [d, $^3J_{HH}$ = 1.6 Hz, 1 H, NCCH], 6.91 [d, $^3J_{HH}$ = 1.6 Hz, 2 H, NCCH], 6.90 [d, $^3J_{HH}$ = 1.6 Hz, 1 H, NCCH), 3.95 [s, 3 H, NCH_3], 3.72 [s, 6 H, NCH_3), 2.36[s, 3 H, CCH_3]. **^{13}C{^{1}H} NMR** (151 MHz, CD_2Cl_2, 25 °C): δ_C = 277.7 [$^1J_{CW}$ = 85 Hz, W≡C], 216.0 [$^1J_{CW}$ = 119 Hz, CO], 187.7 [$^1J_{CW}$ = 90 Hz, NCN], 173.7 [$^1J_{CW}$ = 71 Hz, NCN], 149.6 [$C^{2,6}(C_6H_4)$], 140.4 [$^2J_{CW}$ = 97 Hz, $C^1(C_6H_4)$], 130.3 [$C^{3,5}(C_6H_4)$], 129.5 [$C^4(C_6H_4)$], 124.8 [$C^3(C_3N_2H_2)$], 124.5 [$C^3(C_3N_2H_2)$], 122.0 [$C^4(C_3N_2H_2)$], 121.5 [$C^4(C_3N_2H_2)$], 39.4 [NCH_3], 38.0 [NCH_3], 21.81 [$C_6H_4CH_3$]. **^{11}B{^{1}H} NMR** (128 MHz, CD_2Cl_2, 25 °C): δ_B = −1.60 (BH). **^{11}B NMR** (128 MHz, CD_2Cl_2, 25 °C): δ_B = −1.47 [d, $^1J_{BH}$ = 101.2 Hz, BH]. **MS** (ESI, +ve ion, *m*/*z*): Found: 853.0721. Calcd for $C_{22}H_{23}Au^{11}B^{35}ClN_6O_2{}^{184}W$ 853.0731. $[M + Na]^+$. See Figure 8 for computationally optimized molecular geometry.

4. Conclusions

The first examples of mononuclear and binuclear carbyne complexes ligated by poly(imidazolylidenyl)borates have been isolated. Spectroscopic data for these add to the growing evidence that poly(imidazolylidenyl)borates are particularly strong net donor ligands. These data are contextualised by comparison with those having a wide range of more familiar κ^3, η^5 and η^6 facially capping ligands, with recourse to two parameters k_{CO} and $\%Vol_{bur}$. Reminiscent of the steric/electronic map presented by Tolman to describe the coordinative features of phosphines, a similar map based on k_{CO} and $\%Vol_{bur}$ suggests that $HB(Im^R)_3$ ligands occupy a sparsely populated region of ligand space, associated with potent net basicity and significant (but variable) steric encumbrance.

The first of these parameters, k_{CO} (a Cotton–Kraihanzel force constant), is given by

$$k_{CO}\ [Ncm^{-1}] = 1.7426 \times 10^{-6}\ Ncm \times (\nu_s{}^2 + \nu_{as}{}^2)$$

where ν_s and ν_{as} are the uncorrected frequencies (in cm^{-1}) calculated at the ωB97X-D/6-31G*/LANL2Dζ level of theory for the complexes [W(≡CC_6H_4Me-4)$(CO)_2$(L)] in the gas phase.

The second of these, $\%Vol_{bur}$, is obtained using the *SambVca* protocol [35] applied to either the computationally optimised geometries or, where available, the experimentally determined atomic coordinates with hydrogen atoms included based on a sphere of 3.5Å radius centred on tungsten. Because this approach may be applied to hypothetical as well as real molecules, the method may enjoy predictive value with limited computational expense. For comparison of calculated and experimentally determined infrared data in the region of ν_{CO}-associated vibrations (1850–2100 cm^{-1}), an anharmonic scaling factor of 0.9297 is recommended for the combination of the ωB97X-D functional and 6-31G* basis set.

Supplementary Materials: The following supporting information can be downloaded at: https://www.mdpi.com/article/10.3390/molecules28237761/s1, IR, ^{1}H, ^{13}C{^{1}H} and ^{11}B NMR spectra for new compounds.

Author Contributions: Conceptualization, A.F.H.; methodology, A.F.H.; formal analysis, C.M.I., R.A.M., R.M.K., M.D.S., L.J.W. and A.F.H.; investigation, C.M.I., M.S., R.A.M., M.D.S., R.M.K. and L.J.W.; resources, A.F.H.; data curation, writing, supervision, project administration, and funding acquisition, A.F.H. All authors have read and agreed to the published version of the manuscript.

Funding: This research was funded by the Australian Research Council, grant number DP230199215.

Data Availability Statement: The data presented in this study are available in the accompanying electronic supporting information.

Conflicts of Interest: The authors declare no conflict of interest.

References

1. Trofimenko, S. Boron-pyrazole Chemistry. IV. Carbon- and Boron-Substituted Poly[(1-pyrazolyl) borates]. *J. Am. Chem. Soc.* **1967**, *89*, 6288–6294. [CrossRef]
2. Trofimenko, S. *Scorpionates: The Coordination Chemistry of Polypyrazolylborate Ligands*; Imperial College Press: London, UK, 1999.
3. Pettinari, C. *Scorpionates II: Chelating Borate Ligands*; Imperial College Press: London, UK, 2008.
4. Hopkinson, M.; Richter, C.; Schedler, M.; Glorius, F. An Overview of N-Heterocyclic Carbenes. *Nature* **2014**, *510*, 485–496. [CrossRef] [PubMed]
5. Bellotti, P.; Koy, M.; Glorius, F. Recent Advances in the Chemistry and Applications of N-heterocyclic Carbenes. *Nat. Rev. Chem.* **2021**, *5*, 711–725. [CrossRef] [PubMed]
6. Smith, C.A.; Narouz, M.R.; Lummis, P.A.; Singh, I.; Nazemi, A.; Li, C.-H.; Crudden, C.M. N-Heterocyclic Carbenes in Materials Chemistry. *Chem. Rev.* **2019**, *119*, 4986–5056. [CrossRef] [PubMed]
7. Kernbach, U.; Ramm, M.; Luger, P.; Fehlhammer, W.P. A Chelating Triscarbene and its Hexacarbene Iron Complex. *Angew. Chem. Int. Ed.* **1996**, *35*, 310–312. [CrossRef]
8. Frankel, R.; Kniczek, J.; Ponikwar, W.; Noth, H.; Polborn, K.; Fehlhammer, W.P. Bis(imidazolin-2-ylidene-1-yl)borate Complexes of Palladium(II), Platinum(II) and Gold(I). *Inorg. Chim. Acta* **2001**, *312*, 23–39. [CrossRef]
9. Frankel, R.; Kernbach, U.; Bakola-Christianopoulou, M.; Plaia, U.; Suter, M.; Ponikwar, W.; Noth, H.; Moinet, C.; Fehlhammer, W.P. Hexacarbene Complexes. *J. Organomet. Chem.* **2001**, *617–618*, 530–545. [CrossRef]
10. Biffis, A.; Tubaro, C.; Scattolin, E.; Basato, M.; Papini, G.; Santini, C.; Alvarez, E.; Conejero, S. Trinuclear Copper(I) Complexes with Triscarbene Ligands: Catalysis of C–N and C–C Coupling Reactions. *Dalton Trans.* **2009**, *35*, 7223–7229. [CrossRef]
11. Nieto, I.; Cervantes-Lee, F.; Smith, J.M. A New Synthetic Route to Bulky "Second Generation" Tris(imidazol-2-ylidene)borate Ligands: Synthesis of a Four Coordinate Iron(ii) Complex. *Chem. Commun.* **2005**, *30*, 3811–3813. [CrossRef]
12. Lu, Z.; Williams, T.J. Di(carbene)-Supported Nickel Systems for CO_2 Reduction Under Ambient Conditions. *ACS Catal.* **2016**, *6*, 6670–6673. [CrossRef]
13. Meihaus, K.R.; Minasian, S.G.; Lukens, W.W., Jr.; Kozimor, S.A.; Shuh, D.K.; Tyliszczak, T.; Long, J.R. Influence of Pyrazolate vs N-Heterocyclic Carbene Ligands on the Slow Magnetic Relaxation of Homoleptic Trischelate Lanthanide(III) and Uranium(III) Complexes. *J. Am. Chem. Soc.* **2014**, *136*, 6056–6068. [CrossRef] [PubMed]
14. Hickey, A.K.; Muñoz, S.B.; Lutz, S.A.; Pink, M.; Chen, C.-H.; Smith, J.M. Arrested α-hydride migration activates a phosphido ligand for C–H insertion. *Chem. Commun.* **2017**, *53*, 412–415. [CrossRef] [PubMed]
15. Elpitiya, G.R.; Malbrecht, B.J.; Jenkins, D.M. A Chromium(II) Tetracarbene Complex Allows Unprecedented Oxidative Group Transfer. *Inorg. Chem.* **2017**, *56*, 14101–14110. [CrossRef] [PubMed]
16. Bass, H.M.; Cramer, S.A.; McCullough, A.S.; Bernstein, K.J.; Murdock, C.R.; Jenkins, D.M. Employing Dianionic Macrocyclic Tetracarbenes to Synthesize Neutral Divalent Metal Complexes. *Organometallics* **2013**, *32*, 2160–2167. [CrossRef]
17. Isbill, S.B.; Chandrachud, P.P.; Kern, J.L.; Jenkins, D.M.; Roy, S. Elucidation of the Reaction Mechanism of $C_2 + N_1$ Aziridination from Tetracarbene Iron Catalysts. *ACS Catal.* **2019**, *9*, 6223–6233. [CrossRef]
18. Chandrachud, P.P.; Bass, H.M.; Jenkins, D.M. Synthesis of Fully Aliphatic Aziridines with a Macrocyclic Tetracarbene Iron Catalyst. *Organometallics* **2016**, *35*, 1652–1657. [CrossRef]
19. Anneser, M.R.; Elpitiya, G.R.; Townsend, J.; Johnson, E.J.; Powers, X.B.; DeJesus, J.F.; Vogiatzis, K.D.; Jenkins, D.M. Unprecedented Five-Coordinate Iron(IV) Imides Generate Divergent Spin States Based on the Imide R-Groups. *Angew. Chem. Int. Ed.* **2019**, *58*, 8115–8118. [CrossRef]
20. Anneser, M.R.; Elpitiya, G.R.; Powers, X.B.; Jenkins, D.M. Toward a Porphyrin-Style NHC: A 16-Atom Ringed Dianionic Tetra-NHC Macrocycle and Its Fe(II) and Fe(III) Complexes. *Organometallics* **2019**, *38*, 981–987. [CrossRef]
21. DeJesus, J.F.; Jenkins, D.M. A Chiral Macrocyclic Tetra- *N* -Heterocyclic Carbene Yields an "All Carbene" Iron Alkylidene Complex. *Chem. Eur. J.* **2020**, *26*, 1429–1435. [CrossRef]
22. Nieto, I.; Bontchev, R.P.; Smith, J.M. Synthesis of a Bulky Bis(carbene)borate Ligand—Contrasting Structures of Homoleptic Nickel(II) Bis(pyrazolyl)borate and Bis(carbene)borate Complexes. *Eur. J. Inorg. Chem.* **2008**, *2008*, 2476–2480. [CrossRef]
23. Arrowsmith, M.; Hill, M.S.; Kociok-Köhn, G. Bis(imidazolin-2-ylidene-1-yl)borate Complexes of the Heavier Alkaline Earths: Synthesis and Studies of Catalytic Hydroamination. *Organometallics* **2009**, *28*, 1730–1738. [CrossRef]
24. Kaufhold, S.; Rosemann, N.W.; Chábera, P.; Lindh, L.; Losada, I.B.; Uhlig, J.; Pascher, T.; Strand, D.; Wärnmark, K.; Yartsev, A.; et al. Microsecond Photoluminescence and Photoreactivity of a Metal-Centered Excited State in a Hexacarbene–Co(III) Complex. *J. Am. Chem. Soc.* **2021**, *143*, 1307–1312. [CrossRef]
25. Kjær, K.S.; Kaul, N.; Prakash, O.; Chábera, P.; Rosemann, N.W.; Honarfar, A.; Gordivska, O.; Fredin, L.A.; Bergquist, K.E.; Häggström, L.; et al. Luminescence and reactivity of a charge-transfer excited iron complex with nanosecond lifetime. *Science* **2019**, *363*, 249–253. [CrossRef] [PubMed]

26. Forshaw, A.P.; Smith, J.M.; Ozarowski, A.; Krzystek, J.; Smirnov, D.; Zvyagin, S.A.; Harris, T.D.; Karunadasa, H.I.; Zadrozny, J.M.; Schnegg, A.; et al. Low-Spin Hexacoordinate Mn(III): Synthesis and Spectroscopic Investigation of Homoleptic Tris(pyrazolyl)borate and Tris(carbene)borate Complexes. *Inorg. Chem.* **2013**, *52*, 144–159. [CrossRef]
27. Prakash, O.; Chábera, P.; Rosemann, N.W.; Huang, P.; Häggström, L.; Ericsson, T.; Strand, D.; Persson, P.; Bendix, J.; Lomoth, R.; et al. A Stable Homoleptic Organometallic Iron(IV) Complex. *Chem. Eur. J.* **2020**, *26*, 12728–12732. [CrossRef] [PubMed]
28. Forshaw, A.P.; Bontchev, R.P.; Smith, J.M. Oxidation of the Tris(carbene)borate Complex $PhB(MeIm)_3Mn^{I}(CO)_3$ to $Mn^{IV}[PhB(MeIm)_3]_2(OTf)_2$. *Inorg. Chem.* **2007**, *46*, 3792–3794. [CrossRef]
29. Chen, F.; Wang, G.-F.; Li, Y.-Z.; Chen, X.-T.; Xue, Z.-L. Syntheses, structures and electrochemical properties of homoleptic ruthenium(III) and osmium(III) complexes bearing two tris(carbene)borate ligands. *Inorg. Chem. Commun.* **2012**, *21*, 88–91. [CrossRef]
30. Chen, F.; Wang, G.-F.; Li, Y.-Z.; Chen, X.-T.; Xue, Z.-L. Synthesis and characterization of rhodium(I) and iridium(I) carbonyl phosphine complexes with bis(N-heterocyclic carbene)borate ligands. *J. Organomet. Chem.* **2010**, *710*, 36–43. [CrossRef]
31. Chen, F.; Sun, J.-F.; Li, T.-Y.; Chen, X.-T.; Xue, Z.-L. Iridium(I) and Rhodium(I) Carbonyl Complexes with the Bis(3-*tert*-butylimidazol-2-ylidene)borate Ligand and Unusual B−H Fluorination. *Organometallics* **2011**, *30*, 2006–2011. [CrossRef]
32. Nishiura, T.; Takabatake, A.; Okutsu, M.; Nakazawa, J.; Hikichi, S. Heteroleptic cobalt(iii) acetylacetonato complexes with N-heterocyclic carbine-donating scorpionate ligands: Synthesis, structural characterization and catalysis. *Dalton Trans.* **2019**, *48*, 2564–2568. [CrossRef]
33. Fostvedt, J.I.; Lohrey, T.D.; Bergman, R.G.; Arnold, J. Structural diversity in multinuclear tantalum polyhydrides formed via reductive hydrogenolysis of metal–carbon bonds. *Chem. Commun.* **2019**, *55*, 13263–13266. [CrossRef]
34. Fostvedt, J.I.; Boreen, M.A.; Bergman, R.G.; Arnold, J. A Diverse Array of C–C Bonds Formed at a Tantalum Metal Center. *Inorg. Chem.* **2021**, *60*, 9912–9931. [CrossRef] [PubMed]
35. Nieto, I.; Bontchev, R.P.; Ozarowski, A.; Smirnov, D.; Krzystek, J.; Telser, J.; Smith, J.M. Synthesis and spectroscopic investigations of four-coordinate nickel complexes supported by a strongly donating scorpionate ligand. *Inorganica Chim. Acta* **2009**, *362*, 4449–4460. [CrossRef]
36. Papini, G.; Bandoli, G.; Dolmella, A.; Lobbia, G.G.; Pellei, M.; Santini, C. New homoleptic carbene transfer ligands and related coinage metal complexes. *Inorg. Chem. Commun.* **2008**, *11*, 1103–1110. [CrossRef]
37. Muñoz, S.B.; Foster, W.K.; Lin, H.-J.; Margarit, C.G.; Dickie, D.A.; Smith, J.M. Tris(carbene)borate Ligands Featuring Imidazole-2-ylidene, Benzimidazol-2-ylidene, and 1,3,4-Triazol-2-ylidene Donors. Evaluation of Donor Properties in Four-Coordinate $\{NiNO\}^{10}$ Complexes. *Inorg. Chem.* **2012**, *51*, 12660–13668. [CrossRef] [PubMed]
38. Xu, W.-F.; Li, X.-W.; Li, Y.-Z.; Chen, X.-T.; Xue, Z.-L. Synthesis and structures of π-allylpalladium(II) complexes containing bis(1,2,4-triazol-5-ylidene-1-yl)borate ligands. An unusual tetrahedral palladium complex. *J. Organomet. Chem.* **2011**, *696*, 3800–3806. [CrossRef]
39. Huang, J.; Stevens, E.D.; Nolan, S.P.; Petersen, J.L. Olefin Metathesis-Active Ruthenium Complexes Bearing a Nucleophilic Carbene Ligand. *J. Am. Chem. Soc.* **1999**, *121*, 2674–2678. [CrossRef]
40. Scholl, M.; Trnka, T.M.; Morgan, J.P.; Grubbs, R.H. Increased Ring Closing Metathesis Activity of Ruthenium-Based Olefin Metathesis Catalysts Coordinated with Imidazolin-2-ylidene Ligands. *Tetrahedron Lett.* **1999**, *40*, 2247–2250. [CrossRef]
41. Ackermann, L.; Fürstner, A.; Weskamp, T.; Kohl, F.J.; Herrmann, W.A. Ruthenium carbene complexes with imidazolin-2-ylidene ligands allow the formation of tetrasubstituted cycloalkenes by RCM. *Tetrahedron Lett.* **1999**, *40*, 4787–4790. [CrossRef]
42. Scholl, M.; Ding, S.; Lee, C.W.; Grubbs, R.H. Synthesis and Activity of a New Generation of Ruthenium-Based Olefin Metathesis Catalysts Coordinated with 1,3-Dimesityl-4,5-dihydroimidazol-2-ylidene Ligands. *Org. Lett.* **1999**, *1*, 953–956. [CrossRef]
43. Cardin, D.J.; Doyle, M.J.; Lappert, M.F. Rhodium(I)-catalysed dismutation of electron-rich olefins: Rhodium(I) carbene complexes as intermediates. *J. Chem. Soc. Chem. Commun.* **1972**, *16*, 927–928. [CrossRef]
44. Shao, M.; Zheng, L.; Qiao, W.; Wang, J.; Wang, J. A Unique Ruthenium Carbyne Complex: A Highly Thermo-endurable Catalyst for Olefin Metathesis. *Adv. Synth. Catal.* **2012**, *354*, 2743–2750. [CrossRef]
45. Ledoux, N.; Drozdzak, R.; Allaert, B.; Linden, A.; Van Der Voort, P.; Verpoort, F. Exploring new synthetic strategies in the development of a chemically activated Ru-based olefin metathesis catalyst. *Dalton Trans.* **2007**, *44*, 5201–5210. [CrossRef] [PubMed]
46. Buil, M.L.; Cardo, J.J.F.; Esteruelas, M.A.; Oñate, E. Square-Planar Alkylidyne–Osmium and Five-Coordinate Alkylidene–Osmium Complexes: Controlling the Transformation from Hydride-Alkylidyne to Alkylidene. *J. Am. Chem. Soc.* **2016**, *138*, 9720–9728. [CrossRef] [PubMed]
47. Castarlenas, R.; Esteruelas, M.A.; Lalrempuia, R.; Oliván, M.; Oñate, E. Osmium−Allenylidene Complexes Containing an N-Heterocyclic Carbene Ligand. *Organometallics* **2008**, *27*, 795–798. [CrossRef]
48. Buil, M.L.; Cardo, J.J.F.; Esteruelas, M.A.; Oñate, E. Dehydrogenative Addition of Aldehydes to a Mixed NHC-Osmium-Phosphine Hydroxide Complex: Formation of Carboxylate Derivatives. *Organometallics* **2016**, *35*, 2171–2173. [CrossRef]
49. Castarlenas, R.; Esteruelas, M.A.; Oñate, E. Preparation and Structure of Alkylidene−Osmium and Hydride−Alkylidyne−Osmium Complexes Containing an N-Heterocyclic Carbene Ligand. *Organometallics* **2007**, *26*, 2129–2132. [CrossRef]
50. Buil, M.L.; Cardo, J.J.F.; Esteruelas, M.A.; Fernández, I.; Oñate, E. Hydroboration and Hydrogenation of an Osmium–Carbon Triple Bond: Osmium Chemistry of a Bis-σ-Borane. *Organometallics* **2015**, *34*, 547–550. [CrossRef]

51. Fuchs, J.; Irran, E.; Hrobárik, P.; Klare, H.F.T.; Oestreich, M. Si–H Bond Activation with Bullock's Cationic Tungsten(II) Catalyst: CO as Cooperating Ligand. *J. Am. Chem. Soc.* **2019**, *141*, 18845–18850. [CrossRef]
52. Koy, M.; Elser, I.; Meisner, J.; Frey, W.; Wurst, K.; Kästner, J.; Buchmeiser, M.R. High Oxidation State Molybdenum *N* -Heterocyclic Carbene Alkylidyne Complexes: Synthesis, Mechanistic Studies, and Reactivity. *Chem. Eur. J.* **2017**, *23*, 15484–15490. [CrossRef]
53. Hauser, P.M.; van der Ende, M.; Groos, J.; Frey, W.; Wang, D.; Buchmeiser, M.R. Cationic Tungsten Alkylidyne *N*-Heterocyclic Carbene Complexes: Synthesis and Reactivity in Alkyne Metathesis. *Eur. J. Inorg. Chem.* **2020**, *2020*, 3070–3082. [CrossRef]
54. Elser, I.; Groos, J.; Hauser, P.M.; Koy, M.; van der Ende, M.; Wang, D.; Frey, W.; Wurst, K.; Meisner, J.; Ziegler, F.; et al. Molybdenum and Tungsten Alkylidyne Complexes Containing Mono-, Bi-, and Tridentate *N*-Heterocyclic Carbenes. *Organometallics* **2019**, *38*, 4133–4146. [CrossRef]
55. Groos, J.; Koy, M.; Musso, J.; Neuwirt, M.; Pham, T.; Hauser, P.M.; Frey, W.; Buchmeiser, M.R. Ligand Variations in Neutral and Cationic Molybdenum Alkylidyne NHC Catalysts. *Organometallics* **2022**, *41*, 1167–1183. [CrossRef]
56. Groos, J.; Hauser, P.M.; Koy, M.; Frey, W.; Buchmeiser, M.R. Highly Reactive Cationic Molybdenum Alkylidyne *N*-Heterocyclic Carbene Catalysts for Alkyne Metathesis. *Organometallics* **2021**, *40*, 1178–1184. [CrossRef]
57. Hauser, P.M.; Musso, J.V.; Frey, W.; Buchmeiser, M.R. Cationic Tungsten Oxo Alkylidene *N*-Heterocyclic Carbene Complexes via Hydrolysis of Cationic Alkylidyne Progenitors. *Organometallics* **2021**, *40*, 927–937. [CrossRef]
58. Caldwell, L.M. Alkylidyne Complexes Ligated by Poly(pyrazolyl)borates. *Adv. Organomet. Chem.* **2008**, *56*, 1–94. [CrossRef]
59. Mathur, M.A.; Moore, D.A.; Popham, R.E.; Sisler, H.H.; Dolan, S.; Shore, S.G. Trimethylamine-Tribromoborane. *Inorg. Synth.* **2007**, *29*, 51–54. [CrossRef]
60. Dossett, S.J.; Hill, A.F.; Jeffery, J.C.; Marken, F.; Sherwood, P.; Stone, F.G.A. Synthesis and Reactions of the Alkylidynemetal Complexes [M(CR)(CO)$_2$(η-C$_5$H$_5$)](R = C$_6$H$_3$Me$_2$-2,6, M = Cr, Mo, or W; R = C$_6$H$_4$Me-2, C$_6$H$_4$OMe-2, or C$_6$H$_4$NMe$_2$-4, M = Mo); Crystal Structure of the Compound [MoFe(μ-CC$_6$H$_3$Me$_2$-2,6)(CO)$_5$(η-C$_5$H$_5$)]. *J. Chem. Soc. Dalton Trans.* **1988**, *9*, 2453–2465. [CrossRef]
61. Anderson, S.; Hill, A.F.; Nasir, B.A. Steric and "Indenyl" Effects in the Chemistry of Alkylidyne Complexes of Tungsten and Molybdenum. *Organometallics* **1995**, *14*, 2987–2992. [CrossRef]
62. Hill, A.F.; Malget, J.M.; White, A.J.P.; Williams, D.J. Dihydrobis(pyrazolyl)borate Alkylidyne Complexes of Tungsten. *Eur. J. Inorg. Chem.* **2004**, *2004*, 818–828. [CrossRef]
63. Ghadwal, R.S.; Rottschäfer, D.; Andrada, D.M.; Frenking, G.; Schürmann, C.J.; Stammler, H.-G. Normal-to-abnormal rearrangement of an N-heterocyclic carbene with a silylene transition metal complex. *Dalton Trans.* **2017**, *46*, 7791–7799. [CrossRef] [PubMed]
64. Jeffery, J.C.; Gordon, F.; Stone, A.; Williams, G.K. Synthesis of alkylidyne tungsten complexes with hydrotris(pyrazol-1-yl)borate ligands. *Polyhedron* **1991**, *10*, 215–219. [CrossRef]
65. Anderson, S.; Cook, D.J.; Hill, A.F.; Malget, J.M.; White, A.J.P.; Williams, D.J. Reactions of Tungsten Alkylidynes with Thionyl Chloride. *Organometallics* **2004**, *23*, 2552–2557. [CrossRef]
66. Wadepohl, H.; Arnold, U.; Pritzkow, H.; Calhorda, M.J.; Veiros, L.F. Interplay of ketenyl and nitrile ligands on d6-transition metal centres. Acetonitrile as an end-on (two-electron) and a side-on (four-electron) ligand. *J. Organomet. Chem.* **1999**, *587*, 233–243. [CrossRef]
67. Foreman, M.R.S.-J.; Hill, A.F.; White, A.J.P.; Williams, D.J. Hydrotris(methimazolyl)borato Alkylidyne Complexes of Tungsten. *Organometallics* **2003**, *22*, 3831–3840. [CrossRef]
68. Kläui, W.; Hamers, H. Molybdän- und wolfram-dicarbonyl-carbin-komplexe stabilisiert durch dreizähnige sauerstoff-liganden. *J. Organomet. Chem.* **1988**, *345*, 287–298. [CrossRef]
69. Mayr, A.; Ahn, S. Oxidatively induced insertion of an alkylidyne unit into the tungsten tris(pyrazolyl)borate cage. *Inorganica Chim. Acta* **2000**, *300–302*, 406–413. [CrossRef]
70. Delaney, A.R.; Frogley, B.J.; Hill, A.F. Metal coordination to a dimetallaoctatetrayne. *Dalton Trans.* **2019**, *48*, 13674–13684. [CrossRef]
71. Manzano, R.A.; Hill, A.F. Fluorocarbyne complexes via electrophilic fluorination of carbido ligands. *Chem. Sci.* **2023**, *14*, 3776–3781. [CrossRef]
72. Tolman, C.A. Steric effects of phosphorus ligands in organometallic chemistry and homogeneous catalysis. *Chem. Rev.* **1977**, *77*, 313–348. [CrossRef]
73. Gusev, D.G. Electronic and Steric Parameters of 76 N-Heterocyclic Carbenes in Ni(CO)$_3$(NHC). *Organometallics* **2009**, *28*, 6458–6461. [CrossRef]
74. Dorta, R.; Stevens, E.D.; Hoff, C.D.; Nolan, S.P. Stable, three-coordinate Ni(CO)$_2$(NHC)(NHC= N-heterocyclic carbene) complexes enabling the determination of Ni−NHC bond energies. *J. Am. Chem. Soc.* **2003**, *125*, 10490–10491. [CrossRef] [PubMed]
75. Dorta, R.; Stevens, E.D.; Scott, N.M.; Costabile, C.; Cavallo, L.; Hoff, C.D.; Nolan, S.P. Steric and Electronic Properties of N-Heterocyclic Carbenes (NHC): A Detailed Study on Their Interaction with Ni(CO)$_4$. *J. Am. Chem. Soc.* **2005**, *127*, 2485–2495. [CrossRef] [PubMed]
76. Huynh, H.V. Electronic Properties of N-Heterocyclic Carbenes and Their Experimental Determination. *Chem. Rev.* **2018**, *118*, 9457–9492. [CrossRef] [PubMed]

77. Abernethy, R.J.; Foreman MR, S.t.-J.; Hill, A.F.; Tshabang, N.; Willis, A.C.; Young, R.D. Similar arguments have been applied to complexes of the form [M(NO)(CO)$_2$(L)] and [M(κ^3-C$_3$H$_5$)(CO)$_2$(L)] (M = Mo, W): (b) Poly(methimazolyl)borato Nitrosyl Complexes of Molybdenum and Tungsten. *Organometallics* **2008**, *27*, 4455–4463. [CrossRef]
78. Abernethy, R.J.; Foreman, M.R.S.-J.; Hill, A.F.; Smith, M.K.; Willis, A.C. Relative hemilabilities of H2B(az)2 (az = pyrazolyl, dimethylpyrazolyl, methimazolyl) chelates in the complexes [M(η-C3H5)(CO)2{H2B(az)2}] (M = Mo, W). *Dalton Trans.* **2020**, *49*, 781–796. [CrossRef] [PubMed]
79. Green, M.; Howard, J.A.K.; James, A.L.; Nunn, C.M.; Stone, F.G.A. Alkylidyne(carbaborane)tungsten-gold and -Rhodium Complexes; Crystal Structures of [AuW(μ-CR)(CO)$_2$(PPh$_3$)(η^5-C$_2$B$_9$H$_9$Me$_2$)], [RhW(μ-CR)(CO)$_2$(PPh$_3$)$_2$(η^5-C$_2$B$_9$H$_9$Me$_2$)], and [RhW(μ-CR)(CO)$_2$(PPh$_3$)$_2${η^5-C$_2$B$_9$(C$_7$H$_9$)H$_8$Me$_2$}](R = C$_6$H$_4$Me-4). *J. Chem. Soc. Dalton Trans.* **1987**, *1*, 61–72. [CrossRef]
80. Lee, F.-W.; Chan, M.C.-W.; Cheung, K.-K.; Che, C.-M. Carbyne complexes of the group 6 metals containing 1,4,7-triazacyclononane and its 1,4,7-trimethyl derivative. *J. Organomet. Chem.* **1998**, *552*, 255–263. [CrossRef]
81. Lee, F.-W.; Chan, M.C.-W.; Cheung, K.-K.; Che, C.-M. Synthesis, crystal structures and spectroscopic properties of cationic carbyne complexes of molybdenum and tungsten supported by tripodal nitrogen, phosphorus and sulphur donor ligands. *J. Organomet. Chem.* **1998**, *563*, 191–200. [CrossRef]
82. Fischer, E.O.; Lindner, T.L.; Kreissl, F.R. Übergangsmetall-carbin-komplexe: XVI. π-Cyclopentadienyl(dicarbonyl)carbin-komplexe des wolframs. *J. Organomet. Chem.* **1976**, *112*, C27–C30. [CrossRef]
83. Fischer, E.O.; Lindner, T.L.; Huttner, G.; Friedrich, P.; Kreißl, F.R.; Besenhard, J.O. Übergangsmetall-Carbin-Komplexe, XXVII. Dicarbonyl(π-cyclopentadienyl)carbin-Komplexe des Wolframs. *Eur. J. Inorg. Chem.* **1977**, *110*, 3397–3404. [CrossRef]
84. Green, M.; Howard, J.A.K.; James, A.P.; Nunn, C.M.; Stone, F.G.A. Synthesis of Alkylidynetungsten Complexes with (Pyrazol-1-yl)borato Ligands; Crystal Structures of [W(CC$_6$H$_4$Me-4)(CO)$_2${B(pz)$_4$}], [Rh$_2$W(μ$_3$-CC$_6$H$_4$Me-4)(μ-CO)(CO)$_2$(η-C$_9$H$_7$)$_2${HB(pz)$_3$}]·CH$_2$Cl$_2$ and [FeRhW(μ$_3$-CC$_6$H$_4$Me-4)(μ-MeC$_2$Me)(CO)$_4$(η-C$_9$H$_7$){HB(pz)$_3$}]. *J. Chem. Soc. Dalton Trans.* **1986**, *1*, 187–197. [CrossRef]
85. Green, M.; Howard, J.A.K.; James, A.P.; Jelfs, A.N.d.M.; Nunn, C.M.; Stone, F.G.A. Alkylidyne[pyrazol-1-yl)borato]tungsten complexes:metal–carbon triple bonds as four-electron donors. *J. Chem. Soc. Chem. Commun.* **1984**, *24*, 1623–1625. [CrossRef]
86. Delgado, E.; Hein, J.; Jeffery, J.C.; Ratermann, A.L.; Stone, F.A. Addition of Methylene Groups to the Unsaturated Complex [FeW(μ-CC$_6$H$_4$Me-4)(CO)$_5$(η-C$_5$Me$_5$)]: μ-Alkenyl Ligand Rearrangements at a Dimetal Centre. *J. Organomet. Chem.* **1986**, *307*, C23–C26. [CrossRef]
87. Byers, P.K.; Stone, F.G.A. Alkylidyne Tungsten and Molybdenum Complexes with Pyrazolylmethane Ligands. *J. Chem. Soc. Dalton Trans.* **1990**, *11*, 3499–3505. [CrossRef]
88. Devore, D.D.; Henderson, S.J.; Howard, J.A.; Gordon, F.; Stone, A. Docosahedral carbaboranetungsten-alkylidyne complexes: Synthesis of compounds with heteronuclear metal-metal bonds. *J. Organomet. Chem.* **1988**, *358*, C6–C10. [CrossRef]
89. Crennell, S.J.; DeVore, D.D.; Henderson, S.J.B.; Howard, J.A.K.; Stone, F.G.A. Docosahedral Carbaborane(alkylidyne)tungsten Complexes as Reagents for the Synthesis of Compounds with Heteronuclear Metal–metal Bonds: Crystal Structures of [NEt$_4$][W(CC$_6$H$_6$Me$_2$-2,6)(CO)$_2$(η^6-C$_2$B$_{10}$H$_{10}$Me$_2$)] and [NEt$_4$][WFe(μ-CC$_6$H$_3$Me$_2$-2,6)(CO)$_4$(η^6-C$_2$B$_{10}$H$_{10}$Me$_2$)]. *J. Chem. Soc. Dalton Trans.* **1989**, *7*, 1363–1374. [CrossRef]
90. Cotton, F.A.; Kraihanzel, C.S. Vibrational Spectra and Bonding in Metal Carbonyls. I. Infrared Spectra of Phosphine-substituted Group VI Carbonyls in the CO Stretching Region. *J. Am. Chem. Soc.* **1962**, *84*, 4432–4438. [CrossRef]
91. Parker, D.J. Solvent effects on the infrared active CO stretching frequencies of some metal carbonyl complexes—I. Dimanganese decarbonyl and dirhenium decarbonyl. *Spectrochim. Acta Part A Mol. Spectrosc.* **1983**, *39*, 463–476. [CrossRef]
92. Poater, A.; Cosenza, B.; Correa, A.; Giudice, S.; Ragone, F.; Scarano, V.; Cavallo, L. Samb*V*ca: A Web Application for the Calculation of the Buried Volume of N-Heterocyclic Carbene Ligands. *Eur. J. Inorg. Chem.* **2009**, *2009*, 1759–1766. [CrossRef]
93. Falivene, L.; Cao, Z.; Petta, A.; Serra, L.; Poater, A.; Oliva, R.; Scarano, V.; Cavallo, L. Towards the online computer-aided design of catalytic pockets. *Nat. Chem.* **2019**, *11*, 872–879. [CrossRef]
94. Clavier, H.; Nolan, S.P. Percent buried volume for phosphine and N-heterocyclic carbene ligands: Steric properties in organometallic chemistry. *Chem. Commun.* **2010**, *46*, 841–861. [CrossRef] [PubMed]
95. Chai, J.-D.; Head-Gordon, M. Systematic optimization of long-range corrected hybrid density functionals. *J. Chem. Phys.* **2008**, *128*, 084106. [CrossRef] [PubMed]
96. Chai, J.D.; Head-Gordon, M. Long-range Corrected Hybrid Density Functionals with Damped Atom–atom Dispersion Corrections. *Phys. Chem. Chem. Phys.* **2008**, *10*, 6615–6620. [CrossRef]
97. Hehre, W.J.; Ditchfield, R.; Pople, J.A. Self—Consistent Molecular Orbital Methods. XII. Further Extensions of Gaussian—Type Basis Sets for Use in Molecular Orbital Studies of Organic Molecules. *J. Chem. Phys.* **1972**, *56*, 2257–2261. [CrossRef]
98. Hay, P.J.; Wadt, W.R. Ab initio effective core potentials for molecular calculations. Potentials for the transition metal atoms Sc to Hg. *J. Chem. Phys.* **1985**, *82*, 270–283. [CrossRef]
99. Hay, P.J.; Wadt, W.R. Ab initio effective core potentials for molecular calculations. Potentials for K to Au including the outermost core orbitals. *J. Chem. Phys.* **1985**, *82*, 299–310. [CrossRef]
100. Wadt, W.R.; Hay, P.J. Ab initio effective core potentials for molecular calculations. Potentials for main group elements Na to Bi. *J. Chem. Phys.* **1985**, *82*, 284–298. [CrossRef]
101. *SPARTAN20®*, Wavefunction Inc.: Irvine, CA, USA, 2022.

102. The National Institute of Standards and Technology Computational Chemistry Comparison and Benchmark Data Base. Recommends a scaling factor on 0.9485 for the B97X-D/6-31G* combination. 2022. Available online: https://cccbdb.nist.gov/vibscalejust.asp. (accessed on 20 November 2023).
103. Merrick, J.P.; Moran, D.; Radom, L. An Evaluation of Harmonic Vibrational Frequency Scale Factors. *J. Phys. Chem. A* **2007**, *111*, 11683–11700. [CrossRef]
104. Lin, C.Y.; George, M.W.; Gill, P.M.W. EDF2: A Density Functional for Predicting Molecular Vibrational Frequencies. *Aust. J. Chem.* **2004**, *57*, 365–370. [CrossRef]
105. Halls, M.D.; Velkovski, J.; Schlegel, H.B. Harmonic frequency scaling factors for Hartree-Fock, S-VWN, B-LYP, B3-LYP, B3-PW91 and MP2 with the Sadlej pVTZ electric property basis set. *Theor. Chem. Accounts* **2001**, *105*, 413–421. [CrossRef]
106. Jacobsen, R.L.; Johnson, R.D.; Irikura, K.K.; Kacker, R.N. Anharmonic Vibrational Frequency Calculations Are Not Worthwhile for Small Basis Sets. *J. Chem. Theory Comput.* **2013**, *9*, 951–954. [CrossRef] [PubMed]
107. Barone, V.; Cossi, M. Quantum Calculation of Molecular Energies and Energy Gradients in Solution by a Conductor Solvent Model. *J. Phys. Chem. A* **1998**, *102*, 1995–2001. [CrossRef]
108. Marenich, A.V.; Cramer, C.J.; Truhlar, D.G. Universal Solvation Model Based on Solute Electron Density and on a Continuum Model of the Solvent Defined by the Bulk Dielectric Constant and Atomic Surface Tensions. *J. Phys. Chem. B* **2009**, *113*, 6378–6396. [CrossRef]
109. Klamt, A.; Schüürmann, G. COSMO: A new approach to dielectric screening in solvents with explicit expressions for the screening energy and its gradient. *J. Chem. Soc. Perkin Trans.* **1993**, *2*, 799–805. [CrossRef]
110. Klamt, A. Conductor-like Screening Model for Real Solvents: A New Approach to the Quantitative Calculation of Solvation Phenomena. *J. Phys. Chem.* **1995**, *99*, 2224–2235. [CrossRef]
111. Sokolenko, T.M.; Petko, K.I.; Yagupolskii, L.M. N-Trifluoromethylazoles. *Chem. Heterocyclic Comp.* **2009**, *45*, 430–435. [CrossRef]
112. Maffett, L.S.; Gunter, K.L.; Kreisel, K.A.; Yap, G.P.; Rabinovich, D. Nickel nitrosyl complexes in a sulfur-rich environment: The first poly(mercaptoimidazolyl)borate derivatives. *Polyhedron* **2007**, *26*, 4758–4764. [CrossRef]
113. Green, J.C.; Underwood, C. Pentamethylcyclopentadienylnickelnitrosyl: Synthesis and photoelectron spectrum. *J. Organomet. Chem.* **1997**, *528*, 91–94. [CrossRef]
114. Landry, V.K.; Pang, K.; Quan, S.M.; Parkin, G. Tetrahedral nickel nitrosyl complexes with tripodal [N3] and [Se3] donor ancillary ligands: Structural and computational evidence that a linear nitrosyl is a trivalent ligand. *Dalton Trans.* **2007**, *8*, 820–824. [CrossRef]
115. MacBeth, C.E.; Thomas, J.C.; Betley, T.A.; Peters, J.C. The Coordination Chemistry of "[BP_3]NiX" Platforms: Targeting Low-Valent Nickel Sources as Promising Candidates to L_3NiE and L_3Ni$\dot{\text{E}}$ Linkages. *Inorg. Chem.* **2004**, *43*, 4645–4662. [CrossRef] [PubMed]
116. Tomson, N.C.; Crimmin, M.R.; Petrenko, T.; Roseburgh, L.E.; Sproules, S.; Boyd, W.C.; Bergman, R.G.; DeBeer, S.; Toste, F.D.; Wieghardt, K. A Step Beyond the Feltham-Enemark Notation: Spectroscopic and Correlated Ab Initio Computational Support for an Antiferromagnetically Coupled M(II)(NO) Description of Tp*M(NO)(M = Co, Ni). *J. Am. Chem. Soc.* **2011**, *133*, 18785–18801. [CrossRef] [PubMed]
117. Hoffmann, R.; Chen, M.M.L.; Elian, M.; Rossi, A.R.; Mingos, D.M.P. Pentacoordinate nitrosyls. *Inorg. Chem.* **1974**, *13*, 2666–2675. [CrossRef]
118. Rerek, M.E.; Ji, L.-N.; Basolo, F. The indenyl ligand effect on the rate of substitution reactions of Rh(η-C_9H_7)$(CO)_2$and Mn(η-C_9H_7)$(CO)_3$. *J. Chem. Soc. Chem. Commun.* **1983**, *21*, 1208–1209. [CrossRef]
119. Hart-Davis, A.J.; Mawby, R.J. Reactions of π-indenyl complexes of transition metals. Part I. Kinetics and mechanisms of reactions of tricarbonyl-π-indenylmethylmolybdenum with phosphorus(III) ligands. *J. Chem. Soc. A Inorg. Phys. Theor.* **1969**, 2403–2407. [CrossRef]
120. Bartik, T.; Weng, W.; Ramsden, J.A.; Szafert, S.; Falloon, S.B.; Arif, A.M.; Gladysz, J.A. New Forms of Coordinated Carbon: Wirelike Cumulenic C_3 and C_5 sp Carbon Chains that Span Two Different Transition Metals and Mediate Charge Transfer. *J. Am. Chem. Soc.* **1998**, *120*, 11071–11081. [CrossRef]
121. Manzano, R.A.; Hill, A.F. For a review of tricarbido complexes see Propargylidyne and tricarbido complexes. *Adv. Organomet. Chem.* **2019**, *72*, 103–171. [CrossRef]
122. Cairns, G.A.; Carr, N.; Green, M.; Mahon, M.F. Reaction of [W(η^2-PhC_2Ph)$_3$(NCMe)] with o-diphenylphosphino-styrene and -allylbenzene; evidence for novel carbon–carbon double and triple bond cleavage and alkyne insertion reactions. *Chem. Commun.* **1996**, *21*, 2431–2432. [CrossRef]
123. Yeh, W.-Y. C_{60}-induced alkyne–alkyne coupling and alkyne scission reactions of a tungsten tris(diphenylacetylene) complex. *Chem. Commun.* **2011**, *47*, 1506–1508. [CrossRef]
124. Buss, J.A.; Agapie, T. Four-electron deoxygenative reductive coupling of carbon monoxide at a single metal site. *Nature* **2016**, *529*, 72–75. [CrossRef]
125. Buss, J.A.; Agapie, T. Mechanism of Molybdenum-MediatedCarbon Monoxide Deoxygenation and Coupling: Mono- and Dicarbyne Complexes Precede C−O Bond Cleavage and C−C Bond Formation. *J. Am. Chem. Soc.* **2016**, *138*, 16466–16477. [CrossRef]
126. Buss, J.A.; Bailey, G.A.; Oppenheim, J.; VanderVelde, D.G.; Goddard, W.A.; Agapie, T. CO Coupling Chemistry of a Terminal Mo Carbide: Sequential Addition of Proton, Hydride, and CO Releases Ethenone. *J. Am. Chem. Soc.* **2019**, *141*, 15664–15674. [CrossRef] [PubMed]

127. Bailey, G.A.; Buss, J.A.; Oyala, P.H.; Agapie, T. Terminal, Open-Shell Mo Carbide and Carbyne Complexes: Spin Delocalization and Ligand Noninnocence. *J. Am. Chem. Soc.* **2021**, *143*, 13091–13102. [CrossRef] [PubMed]
128. Ortin, Y.; Lugan, N.; Mathieu, R. Subtle reactivity patterns of non-heteroatom-substituted manganese alkynyl carbene complexes in the presence of phosphorus probes. *Dalton Trans.* **2005**, *9*, 1620–1636. [CrossRef] [PubMed]
129. Casey, C.P.; Kraft, S.; Kavana, M. Intramolecular CH Insertion Reactions of (Pentamethylcyclopentadienyl)Rhenium Alkynylcarbene Complexes. *Organometallics* **2001**, *20*, 3795–3799. [CrossRef]
130. Fischer, E.O.; Chen, J. Nucleophilic Cleavage of the Carbon-Fluorine Bond in a Fluorocarbene Complex of Manganese. *Z. Naturforsch.* **1983**, *38*, 580–581. [CrossRef]
131. Fischer, E.O.; Chen, J.; Scherzer, K. π-Cyclopentadienyl(dicarbonyl)[aryl(halogen)-carben]-komplexe des Mangans und Rheniums. *J. Organomet. Chem.* **1983**, *253*, 231–241. [CrossRef]
132. Orama, O.; Schubert, U.; Kreissl, F.R.; Fischer, E.O. Reaction of a Cationic Carbyne Complex with a Carbonylmetalate. The Phenylketenyl Group as a Bridging Ligand. *Z. Naturforsch.* **1980**, *35*, 82–85. [CrossRef]
133. Young, R.D.; Lawes, D.J.; Hill, A.F.; Ball, G.E. Observation of a Tungsten Alkane σ-Complex Showing Selective Binding of Methyl Groups Using FTIR and NMR Spectroscopies. *J. Am. Chem. Soc.* **2012**, *134*, 8294–8297. [CrossRef]
134. Carter, T.J.; Kampf, J.W.; Szymczak, N.K. Reduction of Borazines Mediated by Low-Valent Chromium Species. *Angew. Chem. Int. Ed.* **2012**, *51*, 13168–13349. [CrossRef]
135. Prinz, R.; Werner, H. Tricarbonylhexamethylborazolechromium. *Angew. Chem. Int. Ed. Engl.* **1967**, *6*, 91–92. [CrossRef]
136. Kreickmann, T.; Arndt, S.; Schrock, R.R.; Müller, P. Imido Alkylidene Bispyrrolyl Complexes of Tungsten. *Organometallics* **2007**, *26*, 5702–5711. [CrossRef]
137. Mathey, F. The Organic Chemistry of Phospholes. *Chem. Rev.* **1988**, *88*, 429–453. [CrossRef]
138. Carmichael, D.; Mathey, F. New Trends in Phosphametallocene Chemistry. *Top. Curr. Chem.* **2002**, *220*, 27–51.
139. Mills, D.P.; Evans, P. f-Block Phospholyl and Arsolyl Chemistry. *Chem. Eur. J.* **2021**, *27*, 6645–6665. [CrossRef] [PubMed]
140. Abel, E.W.; Clark, N.; Towers, C. η-Tetraphenylphospholyl and η-tetraphenylarsolyl derivatives of manganese, rhenium, and iron. *J. Chem. Soc. Dalton Trans.* **1979**, 1552–1556. [CrossRef]
141. Kirk, R.M.; Hill, A.F. Arsolyl-supported intermetallic dative bonding. *Chem. Sci.* **2022**, *13*, 6830–6835. [CrossRef] [PubMed]
142. Kirk, R.M.; Hill, A.F. Free and coordinated biarsolyls. *Dalton Trans.* **2023**, *52*, 13235–13243. [CrossRef]
143. Kirk, R.M.; Hill, A.F. Bridging arsolido complexes. *Dalton Trans.* **2023**, *52*, 10190–10196. [CrossRef]
144. Byers, P.K.; Carr, N.; Stone, F.G.A. Chemistry of polynuclear metal complexes with bridging carbene or carbyne ligands. Part 106. Synthesis and reactions of the alkylidyne complexes [M(CR)$(CO)_2${(C_6F_5)AuC$(pz)_3$}](M = WorMo, R = alkyloraryl, pz = pyrazol-1-yl); crystal structure of [WPtAU$(C_6F_5)(\mu_3$-CMe$)(CO)_2(PMe_2Ph)_2${(C_6F_5)AuC$(pz)_3$}] and 105 preceding parts in the series. *J. Chem. Soc. Dalton Trans.* **1990**, *12*, 3701–3708. [CrossRef]
145. Clark, G.; Cochrane, C.; Roper, W.; Wright, L. The interaction of an osmium-carbon triple bond with copper(I), silver(I) and gold(I) to give mixed dimetallocyclopropene species and the structures of Os(AgCl)(CR)Cl(CO)$(PPh_3)_2$. *J. Organomet. Chem.* **1980**, *199*, C35–C38. [CrossRef]
146. Carr, N.; Gimeno, M.C.; Goldberg, J.E.; PIlotti, M.U.; Stone, F.G.A.; Topiloglu, I. Synthesis of Mixed-metal Compounds via the Salts [NEt_4][Rh(CO)L(η^5-$C_2B_9H_9R_2$)](L = PPh_3, R = H; L = CO, R = Me); Crystal Structures of the Complexes [WRhAu(μ-CC_6H_4Me-4)$(CO)_3(PPh_3)(\eta$-$C_5H_5)(\eta^5$-$C_2B_9H_{11}$)] and [$WRh_2Au_2(\mu_3$-CC_6H_4Me-4$)(CO)_6(\eta$-$C_5H_5)(\eta^5$-$C_2B_9H_9Me_2)_2$]·0.5CH_2Cl_2. *J. Chem. Soc. Dalton Trans.* **1990**, *7*, 2253–2261. [CrossRef]
147. Carriedo, G.A.; Riera, V.; Sánchez, G.; Solans, X. Synthesis of new heteronuclear complexes with bridging carbyne ligands between tungsten and gold. X-Ray crystal structure of [AuW(μ-CC_6H_4Me-4$)(CO)_2$(bipy)(C_6F_5)Br]. *J. Chem. Soc. Dalton Trans.* **1988**, *7*, 1957–1962. [CrossRef]
148. Strasser, C.E.; Cronje, S.; Raubenheimer, H.G. Fischer-type tungsten acyl (carbeniate), carbene and carbyne complexes bearing C5-attached thiazolyl substituents: Interaction with gold(i) fragments. *New J. Chem.* **2010**, *34*, 458–469. [CrossRef]
149. Zhou, X.; Li, Y.; Shao, Y.; Hua, Y.; Zhang, H.; Lin, Y.-M.; Xia, H. Reactions of Cyclic Osmacarbyne with Coinage Metal Complexes. *Organometallics* **2018**, *37*, 1788–1794. [CrossRef]
150. Borren, E.S.; Hill, A.F.; Shang, R.; Sharma, M.; Willis, A.C. A Golden Ring: Molecular Gold Carbido Complexes. *J. Am. Chem. Soc.* **2013**, *135*, 4942–4945. [CrossRef] [PubMed]
151. Frogley, B.J.; Hill, A.F.; Onn, C.S.; Watson, L.J. Bi- and Polynuclear Transition-Metal Carbon Tellurides. *Angew. Chem. Int. Ed.* **2019**, *58*, 15349–15353. [CrossRef] [PubMed]
152. Frogley, B.J.; Hill, A.F. Synthesis of pyridyl carbyne complexes and their conversion to N-heterocyclic vinylidenes. *Chem. Commun.* **2019**, *55*, 15077–15080. [CrossRef] [PubMed]
153. Onn, C.S.; Hill, A.F.; Olding, A. Metal coordination of phosphoniocarbynes. *Dalton Trans.* **2020**, *49*, 12731–12741. [CrossRef]
154. Hill, A.F.; Manzano, R.A. A [C1+C2] Route to Propargylidyne Complexes. *Dalton Trans.* **2019**, *48*, 6596–6610. [CrossRef] [PubMed]
155. Burt, L.K.; Hill, A.F. Heterobimetallic μ_2-Halocarbyne Complexes. *Dalton Trans.* **2022**, *51*, 12080–12099. [CrossRef]
156. Green, M.L.H.; Parkin, G. Application of the Covalent Bond Classification Method for the Teaching of Inorganic Chemistry. *J. Chem. Educ.* **2014**, *91*, 807–816. [CrossRef]
157. Wilford, J.B.; Powell, H.M. The crystal and molecular structure of tricarbonyl-π-cyclopentadienyltungstiotriphenylphosphinegold. *J. Chem. Soc. A Inorganic Phys. Theor.* **1969**, 8–15. [CrossRef]

158. Fischer, P.J.; Krohn, K.M.; Mwenda, E.T.; Young, V.G. (2-(Dimethylammonium)ethyl)cyclopentadienyltricarbonylmetalates: Group VI Metal Zwitterions. Attenuation of the Brønsted Basicity and Nucleophilicity of Formally Anionic Metal Centers. *Organometallics* **2005**, *24*, 5116–5126. [CrossRef]
159. CrysAlisPro. *Oxford Diffraction*; Revision 5.2; Agilent Technologies UK Ltd.: Yarnton, UK, 2013.
160. Dolomanov, O.V.; Bourhis, L.J.; Gildea, R.J.; Howard, J.A.K.; Puschmann, H. OLEX2: A complete structure solution, refinement and analysis program. *J. Appl. Cryst.* **2009**, *42*, 339–341. [CrossRef]
161. Macrae, C.F.; Bruno, I.J.; Chisholm, J.A.; Edgington, P.R.; McCabe, P.; Pidcock, E.; Rodriguez-Monge, L.; Taylor, R.; van de Streek, J.; Wood, P.A. Mercury CSD 2.0—New features for the visualization and investigation of crystal structures. *J. Appl. Crystallogr.* **2008**, *41*, 466–470. [CrossRef]
162. Kuveke, R.E.H.; Barwise, L.; van Ingen, Y.; Vashisht, K.; Roberts, N.; Chitnis, S.S.; Dutton, J.L.; Martin, C.D.; Melen, R. An International Study Evaluating Elemental Analysis. *ACS Cent. Sci.* **2022**, *8*, 855–863. [CrossRef]